Synthetic deconstruction of *hunchback* regulation by Bicoid

Goncalo Fernandes*[1] and Huy Tran*[1,2], Maxime Andrieu[1], Youssoupha Diaw[1], Carmina Perez-Romero[1,3], Cécile Fradin[3], Mathieu Coppey[4], Aleksandra M. Walczak[§2] and Nathalie Dostatni[§1]

[1] Institut Curie, Université PSL, Sorbonne Université, CNRS, Nuclear Dynamics, Paris, France.

[2] Laboratoire de Physique de l'École Normale Supérieure, CNRS, Université PSL, Sorbonne Université, and Université de Paris, Paris, France.

[3] Department of Physics and Astronomy, McMaster University, Hamilton, Canada.

[4] Institut Curie, Université PSL, Sorbonne Université, CNRS UMR168, Laboratoire Physico Chimie Curie, Paris, France.

*Equal contribution

§Corresponding authors: email address: Aleksandra.Walczak@phys.ens.fr; Nathalie.Dostatni@curie.fr

Abstract

During development, cell identity is established reproducibly among individuals through the expression of specific genes at the correct time and correct location in space. How genes extract and combine both positional and temporal information from different transcription factor (TF) profiles along polarity axes remain largely unexplored. Here, we showcase the classic *hunchback* gene in fruit fly embryos, with focus on 3 of its main TFs: Bicoid, Zelda and Hunchback proteins. We constructed a series of synthetic MS2 reporters, where the numbers and combination of binding sites for each TF are varied. Using live imaging of transcription dynamics by these synthetic reporters and modeling tools, we show that *i)* a Bicoid-only synthetic reporter needs 3 more Bicoid binding sites than found in the *hunchback* promoter to recapitulates almost all spatial features of early *hb* expression but takes more time to reach steady state; *ii)* Hunchback and Zelda binding sites combined with Bicoid sites both reduce the time to reach steady state and increase expression at a different step in the activation process: Zld sites lower the Bicoid threshold required for activation while Hb sites increase the polymerase firing rate and reduce bursting; *iii)* the shift of the Bicoid-only reporter induced by a reduction by half of Bicoid concentrations indicates that the decay length of the Bicoid activity gradient is lower than the decay length of the Bicoid protein gradient. Altogether, this work indicates that Bicoid is the main source of positional information for *hunchback* expression and places back the Bicoid system within the physical limits of an equilibrium model.

Introduction

Morphogen gradients are used by various organisms to establish polarity along embryonic axes or within organs. In these systems, positional information stems from the morphogen concentration detected by each cell in the target tissue and mediates the determination of cell identity through the expression of specific sets of target genes. While these processes ensure the reproducibility of developmental patterns and the emergence of properly proportioned individuals, the question of whether the morphogen itself directly contributes to this robustness or whether it requires the involvement of downstream cross-regulatory networks or cell-communication remains largely debated. This question becomes even more pressing with the recent discovery that when studied at the single cell level, transcription is frequently observed to be an extremely noisy process, hardly suggestive of such precise control.

To understand how reproducible transcription patterns can robustly emerge from subtle differences of morphogen concentration, we study the Bicoid (Bcd) morphogen system which initiates pattern

formation along the antero-posterior (AP) axis in the young fruit fly embryo (Driever and Nusslein-Volhard, 1988). As indicated by immuno-fluorescent staining (Houchmandzadeh et al., 2002) and fluorescent tagging (Gregor et al., 2007b), the Bcd gradient is steadily established at the onset of transcription, one hour after egg laying, in the form of an exponential AP gradient with a λ decay length of ~ 20% egg-length (EL). Fluorescent correlation spectroscopy measurements (Abu-Arish et al., 2010) and single molecule tracking of GFP-tagged Bcd proteins (Mir et al., 2018) revealed that a fraction of the Bcd proteins has a fast diffusion coefficient sufficient to explain the establishment of the gradient in such a short time by the synthesis-diffusion-degradation model (Abu-Arish et al., 2010; Fradin, 2017). This was further supported with the use of a tandem fluorescent timer as a protein age sensor (Durrieu et al., 2018). Of note, the establishment of the Bcd gradient is not only rapid but also extremely precise in space with only 10% variability among embryos (Gregor et al., 2007b) and this reproducibility is linearly correlated to the amount of *bcd* mRNA maternally provided and the number of functional *bcd* alleles in the females (Liu et al., 2013; Petkova et al., 2014).

The Bcd protein binds DNA through its homeodomain (Hanes and Brent, 1989; Treisman et al., 1989) and activates the expression of a large number of target genes carrying Bcd binding sites (BS). Among the Bcd target genes, *hunchback* (*hb*) is expressed in a large domain spanning the whole anterior half of the embryo (Driever et al., 1989). *hb* expression begins when the first hints of transcription are detected in the embryo, i.e. at nuclear cycle 8 (Porcher et al., 2010). About one hour later (i.e. at nuclear cycle 14), the expression domain of *hb* is delimited by a posterior boundary, which is both precisely positioned along the AP axis and very steep suggesting that very subtle differences in Bcd concentration in two nearby nuclei at the boundary are already precisely measured to give rise to very different transcriptional responses (Crauk and Dostatni, 2005; Gregor et al., 2007a; Houchmandzadeh et al., 2002). Detailed analysis of *hb* expression by RNA FISH also indicated that transcription at the *hb* locus is extremely dynamic in time: it is detected during the successive S-phases but not during the intervening mitoses, which punctuate this period of development.

To gain insights into the dynamics of *hb* early expression with a higher temporal resolution, the MS2-MCP approach for fluorescent tagging of RNA (Ferraro et al., 2016) was adapted to living fruit fly embryos (Lucas et al., 2013; Garcia et al., 2013). This provided an hb-P2 MS2-reporter expressed anteriorly in a domain with a boundary of the same steepness and positioning precision as the endogenous *hb* (Lucas et al., 2018). Of note, despite, this precise measurement of positional information (position and steepness of the boundary), transcription dynamics showed 150 % of noise among nuclei when measuring the relative production of mRNA (δmRNA/mRNA) at the boundary position (Desponds et al., 2016). This high variability was consistent with smFISH data measuring the variability of *hb* mRNA amounts in nuclei (Little et al., 2013) and reflected a stochastic transcription process in neighboring nuclei which nevertheless all make the precise decision to turn ON *hb* during the cycle.

The transcription dynamics of the hb-P2 MS2-reporter indicated that its steep boundary is established at each nuclear cycle 11 to 13 within 180 seconds and therefore suggested that accurate measurements of Bcd concentration were made much more rapidly than anticipated (Lucas et al., 2018). Modeling was used to recapitulate the observed dynamics assuming cooperative binding of Bcd proteins to the 6 known BS sites of the hb-P2 promoter and rate limiting concentrations of Bcd at the boundary (Tran et al., 2018). The model was able to recapitulate the fast temporal dynamics of the boundary establishment but could not reproduce its observed steepness which, given the 20% EL decay length of the Bcd gradient, corresponds to a Hill coefficient of ~ 7, difficult to achieve without invoking the need for additional energy expenditure (Estrada et al., 2016). As expected, the performance of the model was higher when increasing the number of Bcd BS above 6 with a minimum of 9 Bcd BS required to fit the experimental data with a boundary of the appropriate steepness. This indicated that either the hb-P2 promoter contained more than 6 Bcd BS or that additional mechanisms were required to account for the steepness of the boundary.

Here, we chose a synthetic approach to decipher the functioning of Bcd in the transcription process at the mechanistic level. We built Bcd-only reporters with specific numbers of Bcd BS as well as reporters

with 6 Bcd BS in combination with BS for the two known maternal Bcd co-factors binding to the hb-P2 promoter, namely the Hb protein itself (Porcher et al., 2010; Simpson-Brose et al., 1994) and the Zld pioneer transcription factor (Hannon et al., 2017; Xu et al., 2014). We show that 6 Bcd BS are not sufficient to recapitulate the hb-P2 expression dynamics while a reporter with only 9 Bcd BS recapitulates most of its spatial features, except a slightly lower steepness of its expression boundary and a longer period to reach steady state. To account for the bursty behavior of Bcd-only reporters in excess of Bcd, we fitted our data to a model involving a first step of Bcd binding/unbinding to the BS array and a second step where the bound Bcd molecules activate transcription. Synthetic reporters combining Bcd BS with either Hb or Zld BS indicated that both Hb and Zld sites reduce the time to reach steady state and increase expression by different means: Zld sites contribute to the first step of the model by drastically lowering the Bcd concentration thresholds required for activation while Hb sites act in the second step by reducing Bcd-induced burstiness and increasing the polymerase firing rates. Lastly, the boundary shift of the Bcd-only synthetic reporter with 9 Bcd BS in embryos maternally expressing one (1X) *vs* two (2X) *bcd* functional copies was smaller than the expected shift given the decay length of the Bcd concentration gradient. Thus, we propose the existence of an effective Bcd-activity gradient underlying the Bcd-protein gradient. Altogether, this work reinforces the notion that the Bcd gradient is the main source of positional information for the early expression of *hb* while both Zld and Hb accelerate the process.

Results

Nine Bicoid binding sites alone recapitulate most features of the hb-P2 pattern

We first investigated the transcription dynamics of Bcd-only MS2 reporters carrying exclusively 6, 9 or 12 strong Bcd binding sites (BS) (Hanes and Brent, 1989; Treisman et al., 1989) upstream of an hsp70 minimal promoter (Table S1), all inserted at the same genomic location. Movies were recorded and analyzed from nuclear cycle 11 (nc11) to 13 (nc13) but we focused on nc13 data, which are statistically stronger given the higher number of nuclei analyzed. Unless otherwise specified, most conclusions were also valid for nc11 and nc12.

The expression of the B6 (6 Bcd BS), B9 (9 Bcd BS) and B12 (12 Bcd BS) reporters (Fig. 1A) harbored similar features as expression of the hb-P2 reporter (Lucas et al., 2018), which carries the ~300 bp of the hb-P2 promoter and the *hb* intron (Fig. 1B, Table S1): during the cycle, transcription was first initiated in the anterior with the expression boundary moving rapidly towards the posterior to reach a stable position into nc13 (Fig. 1C). For all synthetic reporters, the mean onset time of transcription T_0 following mitosis (Fig. 1D) showed a dependence on position along the AP axis, as observed for hb-P2 (Lucas et al., 2018). Thus, Bcd concentration is a rate-limiting factor for the expression of all reporters. As indicated by the distributions of onset time T_0 in the anterior (~-30 %EL), the first transcription initiation time at high Bcd concentration were not statistically different (p-values > 0.5) for all synthetic reporters (B6, B9 or B12) and hb-P2 (Fig. 1E). In contrast, in the middle of the axis where Bcd is limiting, transcription dynamics of the various reporters was quite diverse (Fig. 1F): the time it took for the hb-P2 reporter to reach the final decision to position its boundary (converging time, Table S2) was only 225 ± 25 s while it took about twice as much time for B6 (425 ± 25 s) or B9 (475 ± 25 s) and slightly less for B12 (325 ± 25 s).

For all reporters, the fraction of nuclei with MS2 signal during the cycle exhibited a sigmoid-like pattern along the AP axis reaching 100% in the anterior and 0% in the posterior (Fig. 1G). We fitted these patterns with sigmoid functions of position along the AP axis and extracted (see Materials & Methods, section C for derivation) quantitative values for the position and width of the expression boundary (Fig. 1E). Increasing the number of Bcd BS from 6 to 9, shifted the expression boundary towards the posterior and decreased the width of the boundary (Fig. 1H) whereas increasing the number of Bcd sites from 9 to 12 did not significantly change the boundary position nor the boundary width. Of note,

B9, B12 and hb-P2 expression boundaries were at almost identical positions while the width of the hb-P2 boundary was smaller than the width of the B9 or the B12 boundaries (Fig. 1H).

Thus, even though 6 Bcd BS have been described in the hb-P2 promoter, having only 6 Bcd BS alone in a synthetic reporter is not sufficient to recapitulate the *hb* pattern. Increasing this number up to 9 is sufficient to recapitulate almost all spatial features of the hb-P2 pattern except for the steepness of the expression boundary. Of note, the Bcd-only reporters take much longer than the hb-P2 reporter to reach the final decision for boundary positioning suggesting that binding of additional transcription factors in the hb-P2 promoter likely contribute to speeding-up the process.

Bicoid-dependent transcription is bursty at steady state even in excess of Bicoid

To study the kinetics of transcription induced by Bcd, we compared the dynamics of transcription of the hb-P2 and the Bcd-only reporters at steady state (in the time window of 600-800s). From the time trace of MS2 activity in each nucleus, the fluctuation of the transcription process (burstiness) at a given position along the AP axis was featured by P_{Spot}, the average fraction of the cycle length during which fluorescent spots were observed (Fig. 2A). In the anterior (~-30 %EL), P_{Spot} increased when increasing the number of Bcd BS in synthetic reporters from 6 to 9, with $P_{Spot}(B6)$ = 0.47 ± 0.02 and $P_{Spot}(B9)$ = 0.80 ± 0.07. P_{Spot} (*hb-P2*) = 0.84 ± 0.008 was as high as for B9 or B12 ($P_{Spot}(B12)$= 0.76 ± 0.07). These values were all smaller than the fraction of expressing nuclei (~ 1, Fig. 1G). This indicated bursty transcription activity in individual nuclei for all reporters, as confirmed by their individual MS2 traces in this region. Interestingly, P_{Spot} for all Bcd-only reporters reach a plateau in the anterior where the Bcd concentration is in excess (Fig. 2A). Thus, as in this region the Bcd BS on those reporters are likely to be always occupied by Bcd molecules, the burstiness observed is not caused by the binding/unbinding of Bcd to the BS array but by downstream processes. Meanwhile, the mean intensity of the MS2 signals (μ_I) in the anterior region did not vary between reporters (Fig. 2B), suggesting that the number of bound Bcd molecules does not regulate the RNAP firing rate within transcription bursts.

A model to recapitulate expression dynamics from Bicoid-only synthetic reporters

To explain the observed dynamics of the expression patterns (Fig. 1C) and bursty transcription in regions with excess Bcd (Fig. 2A), we built a model for transcription regulation of the Bcd-only synthetic reporters (Fig. 2, C-D). In this model, regulation occurs in two steps: first, nuclear Bcd molecules can bind to and unbind from the Bcd BS on the promoter (Fig. 2C) and second, bound Bcd molecules can activate transcription (Fig. 2D).

In step 1 (Fig. 2C), the binding and unbinding of Bcd to an array of N identical Bcd BS were modeled explicitly, as in (Estrada et al., 2016; Tran et al., 2018). In our model, the binding state is denoted by S_i, with i the number of bound Bcd molecules ($i \leq N$). The binding rate constants k_i depend on the number of free BS ($N - i + 1$) and the Bcd search rate for a single BS k_b. The unbinding rate constants k_{-i} were varied to account for various degrees of Bcd-DNA complex stability and binding cooperativity. In step 2 (Fig. 2D), we expanded this model to account for the burstiness in transcription uncoupled with Bcd binding/unbinding (Fig. 2B). The promoter dynamics was modeled as a two-state model, ON and OFF, to account for the observed bursts of transcription with a moderate time scale (between 10 s and 100 s (Bothma et al., 2014; Desponds et al., 2016; Lammers et al., 2019)). The turning ON rate $k_{ON}(S_i)$ was modulated by i the number of bound Bcd molecules. When the BS arrays had less than K Bcd molecules ($K \geq 0$), transcription could not be activated ($k_{ON}(S_{i<K}) = 0$). To account for the uncoupling between the burstiness of transcription and the Bcd binding and unbinding, the turning OFF rate k_{OFF} did not depend on the Bcd BS state. When the promoter is ON, RNAP could initiate transcription and be fired at rate ρ_{RNAP}. At any given time t and nuclei position x along the AP axis,

we could calculate the probability for the promoter to be in the ON state (see Materials & Methods section D).

In this model, each kinetic parameter could be tuned independently to control the measured transcription dynamics features: Bcd binding rate constants (k_i, k_b) controlled the pattern boundary position, Bcd unbinding rate constants (k_{-i}) controlled the pattern steepness (Estrada et al., 2016; Tran et al., 2018), the activation/deactivation rates (k_{ON}, k_{OFF}) controlled the fraction of active loci during steady state (P_{Spot}), and the RNAP firing rate (ρ_{RNAP}) controlled the mean loci intensity (μ_I). The fit of the model for each Bcd-only reporter with the data is shown Fig. 2 (E-G). By comparing features of the transcription dynamics among Bcd-only reporters, we identified which parameters and consequently which processes were dependent on the number of Bcd BS. We started with the parameters allowing a best fit of the model with the B6 data and allowed each of the parameters to vary, either alone or in combination, to fit the B9 and B12 data. These simulations indicated that very good fits could be obtained for B9 and B12 by allowing only 3 of the k_{-i} parameters to vary (k_{-1}, k_{-2} & k_{-6}) (Fig. S4) while the other parameters remained those identified for B6. Also, as they have more Bcd BS than B6, the fitting of the B9 and B12 data to the model generated new parameters (i.e. $k_{ON}(S_N)$) for N>6).

Given that the expression patterns of hb-P2 and all Bcd-only reporters reached a plateau in the anterior where Bcd concentration is likely in excess, we compared the activation rates $k_{ON}(S_N)$ of the promoter when N = 6, 9 or 12 Bcd BS were occupied. Assuming that the number of bound Bcd proteins did not affect the switch OFF rate k_{OFF}, we found a fold change of ~4.51 between $k_{ON}(S_9)$ and $k_{ON}(S_6)$. This fold change is 3 times greater than the ratio of the Bcd BS numbers between B9 and B6, arguing against independent activation of transcription by individual bound Bcd TF. This analysis detailed in Materials & Methods section G provides evidence for synergistic effects between several bound Bcd molecules.

Hunchback reduces the burstiness of Bicoid-dependent transcription

Despite the same number of Bcd BS in the B6 and hb-P2 reporters, their expression pattern and dynamics were very different (Fig. 1 and Fig. 2A). To determine whether this difference could be explained by the presence of BS for other TFs in the hb-P2 promoter (Fig. 1A), we used our synthetic approach to decipher the impact on the various features highlighted in our model when adding to the reporters BS for the two major partners of Bcd, Hb and Zld also present in hb-P2 promoter (Fig. 3A). As our goal was to determine to which mechanistic step of our model each of these TF contributed, we purposefully started by adding BS numbers that are much higher than in the hb-P2 promoter.

We first analyzed the impact of combining the Bcd BS with Hb BS. A H6 reporter containing only 6 Hb BS did not exhibit any MS2 signal from nc11 to nc13 (not shown). This indicated that the Hb protein alone, even with an abundance of Hb sites, could not activate transcription on its own. When combining 6 Hb BS with the 6 Bcd BS of B6 (henceforth named the H6B6 reporter, Fig. 3A), expression was detected in a similar domain to that of the B6 reporter, albeit with much higher fraction of active loci at any given time during the cycle (Fig. 3B, middle panel). Across the embryo AP axis, the mean onset time of transcription after mitosis T_0 with the H6B6 reporter was not changed (p-values > 0.5) when compared to B6 (Fig. 3C) and in the anterior region (excess of Bcd), the cumulative distribution of onset time T_0 was the same (Fig. 3D). Interestingly, at their respective boundary positions where the Bcd concentration is limiting, the presence of Hb BS reduced to 325 ± 25 s the time required for the synthetic H6B6 reporter to reach the final decision to position its boundary (purple dashed line in Fig. 3E and converging time, Table S2) when it was 425 ± 25 s for B6 (yellow dashed line in Fig. 3I and converging time, Table S2). For H6B6, the fraction of nuclei with MS2 signal during the cycle exhibited a sigmoid-like pattern (Fig. 3F) with, when compared to B6, a boundary slightly (only one nucleus length) shifted towards the posterior and a width reduced by half (Fig. G). The kinetics of transcription regulation by the Hb protein was inferred from the fraction of the loci's active time (P_{Spot}) at steady state. In the anterior region, this fraction was always near-saturation for the H6B6 reporter (~0.95 to

1) (Fig. 3H), with very few nuclei exhibiting bursty expression. This non-bursty behavior of the H6B6 reporter contrasts with the highly bursty expression of B6 reporter. Meanwhile, in the anterior region, the mean fluorescence intensity of active H6B6 loci was at least twice higher than that of all synthetic Bcd-only reporters (Fig. 3I).

To model H6B6 activity, the same formalism, as applied to B9 and B12 reporters, was used starting from the parameter values imposed from the fitted model of B6 and then varying those parameters, either alone or in combination, to fit the H6B6 data. The simulations indicated that a moderate fit to the data was obtained when varying only the k_{ON} and k_{OFF} parameters while varying in addition the 3 of the k_{-i} parameters (k_{-1}, k_{-2} & k_{-6}) allowed very good fitting of the model to the data (Fig. S4).

Altogether, this suggests that Hb binding to the promoter accelerates the measurement of positional information by Bcd by improving both the unbinding kinetics of Bcd to its BS, which is consistent with the half reduction of the boundary steepness (Fig. 3G) and the kinetics of activation/deactivation transcription rates, consistent with reduced burstiness (Fig. 3H).

Zelda lowers the Bcd threshold required for expression

As the hb-P2 promoter also contains Zld BS, we used our synthetic approach to investigate the role of Zld in the Bcd system. a reporter with only 6 Zld BS (Z6) was strongly expressed along the whole AP axis (Fig. S3A), we had to reduce the number of Zld BS in our synthetic approach to analyze Zld effect. A Z2 reporter containing only 2 Zld BS did not exhibit any MS2 signal (not shown). The Z2B6 reporter, combining 2 Zld BS with 6 Bcd BS (Fig. 3A), exhibited a very different expression pattern when compared to B6 (Fig. 3B, right panel). This expression pattern also varied with the nuclear cycles likely because of drastic changes in Zld transcriptional activity (Fig. S3) but for simplicity, we focused here on nc13. The onset time T_0 of the Z2B6 reporter was similar in the anterior to those of the B6, H6B6 and hb-P2 reporters (Fig. 3, C-D) but unlike B6, H6B6 and hb-P2 it did not vary along the AP axis (Fig. 3C). This suggest that Zld binding can accelerate Bcd-dependent transcription when Bcd is rate-limiting but has no effect when Bcd is in excess (Fig. 3C). As observed with H6B6, the presence of Zld BS reduced to 300 ± 25 s the time required for the synthetic Z2B6 reporter to reach the final decision to position its boundary (blue dashed line in Fig. 3E and converging time, Table S2) when it was 425 ± 25 s for B6 (yellow dashed line in Fig. 3E and converging time, Table S2).

The most striking feature of the Z2B6 reporter was the drastic posterior shift of its expression boundary (17.5 %EL) when compared to B6 (Fig. 3C-D). It indicates that the threshold of Bcd concentration required for activation is lowered when two Zld BS are present in the promoter together with 6 Bcd BS. Added to this, the pattern boundary width (Fig. 3G) and in the anterior, both the active loci fraction P_{Spot} (Fig. 3H) and the loci intensity μ_I (Fig. 3I) were very similar for the Z2B6 and B6 reporters. Therefore, we hypothesize that adding 2 Zld sites can accelerate and facilitate Bcd binding when Bcd is rate-limiting (i.e. increasing k_b or k_i) without affecting the remaining parameters (k_{-i}, k_{ON}, k_{OFF}, ρ_{RNAP}). Consistent with this hypothesis, simulations for best fitting of the model to the data, starting from the parameters imposed by B6, indicate that a very good fit of the model to the Z2B6 data is obtained when only varying the Bcd binding rate k_b (Fig. S4).

Altogether, this suggests that Zld binding to the promoter accelerates the measurement of positional information by Bcd by facilitating Bcd binding when it is rate-limiting through an increase of the Bcd binding rate k_b, without affecting the kinetics of activation/deactivation transcription rates.

A Bcd-activity gradient different from the Bcd-protein gradient

Even though Hb is asymmetrically distributed along the AP axis, the presence of Hb BS in our synthetic reporters had only a very mild effect on the positioning of the expression boundary and thus on measurements of positional information by Bcd. Meanwhile, Zld is homogeneously distributed along

the AP axis. Therefore, neither Zld nor Hb could provide strong sources of positional information along the AP axis, leaving the Bcd gradient as the principal source. Our synthetic Bcd-only reporters, which exclusively responded to Bcd, provided the tools to quantitatively and directly test if the position of their expression boundary was exclusively dependent on specific thresholds of Bcd concentration. For this, we reduced the amount of the Bcd protein by half in embryos from females, which were heterozygous for a CRISPR-induced deletion of the *bcd* gene (*⊿bcd*) (see Materials & Methods, section A). As the amount of Bcd protein is produced from each *bcd* allele independently of any other allele in the genome (Liu et al., 2013) and as changing the genetic dosage of *bcd* in the female leads to proportional changes in both mRNA and protein number in the embryo (Petkova et al., 2014), we assumed that embryos from wild-type females (2X) express quantitatively twice as much Bcd proteins as embryos from *⊿bcd*/+ females (1X). In such Bcd-2X and Bcd-1X embryos, we compared the fraction of nuclei expressing the B9 reporter along the AP axis as modeled at the top of Fig. 4A. For simplicity, we denoted $f_{2X}(x)$ the expression pattern in Bcd-2X embryos and $f_{1X}(x)$ the expression pattern in Bcd-1X embryos, with x being the nuclei position along the AP axis.

To quantify the effects of perturbing the Bcd gradient, we first extracted from the experimental data the shift in position $\Delta(x)$ between two nuclei columns with the same expression distribution in Bcd-2X embryos ($f_{2X}(x)$) and in Bcd-1X embryos ($f_{1X}(x-\Delta(x))$, such that $f_{2X}(x) = f_{1X}(x-\Delta(x))$ (Fig. 4B). As all the expression patterns are noisy, we calculated the probability distribution of seeing a given shift $P(\Delta(x)|x)$ for each given position x from our data and used a grey-scale log-probability map as a function of x and Δ to present our results. An example of the log-probability map for the shift expected if the Bcd concentration was reduced by half at each position is shown at the bottom of Fig. 4A. As expected, the prediction of $\Delta(x)$ is most reliable in the boundary region (see Materials & Methods section E for a detailed formulation). From the log-probability map of the shift $\Delta(x)$ obtained from expression data of the B9 reporter in Bcd-2X *vs* Bcd-1X embryos, we observed that the shift in this zone can be described by a constant value $\Delta(x) = \widetilde{\Delta}$ and thus the Bcd gradient measured in this region was exponential. From the data, the best fit value of $\widetilde{\Delta}$ was found to be 10.5 ± 1.0 %EL (cyan dashed line in Fig. 4C). If the threshold of Bcd concentration measured by the Bcd-only reporters was based on the concentration gradient with a decay length $\lambda_{detected}$ ~20% (Gregor et al., 2007b; Houchmandzadeh et al., 2002), the expected shift of the patterns would be $|\Delta_{Expected}| = \lambda_{detected}.ln2$ ~14 %EL (red dashed lines in Fig. 4C). Thus, the fitted shift $|\widetilde{\Delta}|$ ~10.5 %EL extracted from our data is significantly smaller than the expected shift from our knowledge of the Bcd gradient. Of note, the shift obtained at nc13 was larger than the shift obtained at nc12. However, the short length of nc12 (shorter than the time required for the Bcd-only reporters to reach steady state) likely introduces a bias in those measurements (Fig. S5A).

Since the synthetic Bcd-only reporters are expected to position their boundary at the same threshold of active Bcd concentration in Bcd 2X vs Bcd 1X embryos, we propose that they learn about the nuclei position from a gradient of active protein (effective Bcd gradient) rather than from a gradient of concentration detected by immunofluorescence or with GFP-tagged protein, which might include both active and inactive detectable proteins. The effective gradient highlighted by our analysis would be exponential with an effective decay length $\lambda_{eff} = |\widetilde{\Delta}|/ln2$ = 15 ± 1.4 %EL. We projected the decay length for this effective gradient in the model accounting for the pattern dynamics of B9 in Bcd-2X embryos to predict its pattern in Bcd-1X embryos. The predicted patterns from the model (black dashed curves) match well with the data (yellow curves) (Fig. 4B).

Lastly, the comparison of hb-P2 patterns in Bcd-2X and Bcd-1X embryos indicated a shift of 11.0 ± 0.5 %EL of the expression boundary (Fig. 4E). As this value was indistinguishable from the shift $|\widetilde{\Delta}|$ obtained with data of the B9 reporter which only responds to Bcd (Fig. 4E), we concluded that the measure of positional information by the hb-P2 promoter is based entirely on the effective Bcd gradient with λ_{eff} ~15 ± 1.4 %EL and does not involve input from other TF binding to the hb-P2 promoter.

Of note, the shift obtained for the hb-P2 MS2 reporter was significantly larger than the shift of 8% EL described for *hb* in previous studies using the *bcd*^{E1} amorphic allele (Houchmandzadeh et al., 2002; Porcher et al., 2010). To understand this discrepancy, we measured the shift in the boundary positions of our hb-P2 and synthetic MS2 reporters in embryos from wild-type vs *bcd*^{E1}/+ females and confirmed that in this genetic background the shift of boundary position was 8% EL (Fig. 4F and S5B). As the molecular lesion in the *bcd*^{E1} allele introduces a premature stop codon downstream of the homeodomain (Struhl et al., 1989), these results suggest that the *bcd*^{E1} allele likely allows the expression of a weakly functional truncated protein.

The hb-P2 pattern steepness can be explained by an equilibrium model of concentration sensing

Assuming that nuclei extract positional information from an effective Bcd gradient with decay length $\lambda_{eff} < \lambda_{detected}$, we reassessed the Hill coefficient (denoted as H), which reflects the cooperativity of *hb* regulation by Bcd (Estrada et al., 2016; Gregor et al., 2007a). For this, we fitted the pattern of expressing nuclei by the hb-P2 reporters (Fig. 1D) to a sigmoid function. We transformed the fitted sigmoid function of position to a Hill function describing the transcription regulation function of hb-P2 by the Bcd protein concentration (see Materials & Methods section C for detailed formulations). Given the sigmoid function obtained from the data, the inferred Hill coefficient H is proportional to assumed decay length λ (black line in Fig. 5A). Taking the observed effective decay length λ_{eff} = 15 % EL, we obtain H ~ 5.2 compared to H ~ 6.9 for a decay length $\lambda_{detected}$ = 20 %EL. As the hb-P2 promoter contains only 6 known Bcd BS, the value of H = 5.2 for the Hill coefficient inferred assuming the decay length λ_{eff} is now within the limit of concentration sensing with 6 Bcd BS (H = 6, dashed horizontal line in Fig. 5A) while the former value H ~ 6.9 was not achievable without energy expenditure (Estrada et al., 2016) or positive feedback from Hb protein (Lopes et al., 2011).

To verify whether both the dynamics and sharpness of the hb-P2 expression pattern can be sufficiently explained by an equilibrium model of Bcd concentration sensing via N=6 Bcd BS, we fitted our model (Fig. 2) to the kymograph of transcription dynamics by hb-P2 reporter (Fig. 1C). The effects of Hb and Zld are modeled implicitly by the kinetic rate constants. We varied the decay length λ for the Bcd gradient varying from 10 to 20 %EL (model assumptions in Materials & Methods, section F). The model assuming $\lambda = \lambda_{eff}$ = 15 %EL fitted the data significantly better (p-val<0.05) (Fig. 5B) and reproduced a closer Hill coefficient at steady state (Fig. 5A) than the model assuming $\lambda = \lambda_{detected}$ = 20 %EL.

Thus, lowering the decay length of the Bcd gradient to its effective value allows a more reliable fit of the model to the data and places back the Bcd system within the physical limits of an equilibrium model for concentration sensing.

Discussion

In this work, we used a synthetic approach with the focus on cis-regulatory elements, to decipher the kinetics of transcription regulation downstream of the Bcd morphogen gradient in early *Drosophila* embryogenesis. The number and placement of TF BS in our MS2 reporters are not identical to those found on the endogenous *hb* promoter. Nevertheless, this synthetic approach combined with quantitative analyses and modeling sheds light on the mechanisms of transcription regulation by Bcd, Hb and Zld. Based on this knowledge from synthetic reporters, we built the equilibrium model of transcription regulation which agrees with the data from the hb-P2 reporter expression. Therefore, we expect that the mechanisms uncovered are relevant to the patterning of the endogenous *hb* gene.

Expression from the Bcd-only synthetic reporters indicate that increasing the number of Bcd BS from 6 to 9 shifts the transcription pattern boundary position towards the posterior region. This is expected as an array with more BS will be occupied faster with the required amount of Bcd molecules. Increasing the number of Bcd BS from 6 to 9 strongly increases the steepness of the boundary indicating that cooperativity of binding, or more explicitly a longer time to unbind is supported by our model fitting

and likely to be at work in this system. Adding 3 more BS to the 9 Bcd BS has very limited impact, indicating that either Bcd molecules bound to the more distal BS may be too far from the TSS to efficiently activate transcription or that the system is saturated with a binding site array occupied with 9 Bcd molecules. In the anterior with excess Bcd, the fraction of time when the loci are active at steady state also increases when adding 3 Bcd BS from B6 to B9. By assuming a model of transcription activation by Bcd proteins bound to target sites, we found that the activation rate increases by much greater fold (~4.5 times) than the number of BS (1.5 to 2 times) suggesting a synergistic effect in transcription activation by Bcd.

The burstiness of the Bcd-only reporters in regions with saturating amounts of Bcd, led us to build a model in two steps. The first step of this model accounts for the binding/unbinding of Bcd molecules to the BS arrays. It is directly related to the positioning and the steepness of the expression boundary and thus to the measurement of positional information. The second step of this model accounts for the dialog between the bound Bcd molecules and the transcription machinery. It is directly related to the fluctuation of the MS2 signals including the number of firing RNAP at a given time (intensity of the signal) and bursting (frequency and length of the signal). Interestingly, while the first step of the process is achieved with an extreme precision (10% EL) (Gregor et al., 2007a; Porcher et al., 2010), the second step reflects the stochastic nature of transcription and is much noisier (150%) (Desponds et al., 2016; Little et al., 2013). Our model therefore also helps to understand and reconcile this apparent contradiction in the Bcd system.

As predicted by our original theoretical model (Lucas et al., 2018), 9 Bcd BS in a synthetic reporter appear sufficient to reproduce experimentally almost entirely the spatial features of the early *hb* expression pattern i.e. measurements of positional information. This is unexpected as the hb-P2 promoter is supposed to only carry 6 Bcd BS and leaves open the possibility that the number of Bcd BS in the *hb* promoter might be higher, as suggested previously (Park et al., 2019). In addition, while the B9 reporter recapitulates most spatial features of the hb-P2 reporter, it is twice slower to reach the final boundary position in the cycle than the hb-P2 reporter. This suggested that other maternally provided TFs binding to the hb-P2 promoter contribute to fast dynamics of the *hb* pattern establishment. Among these TFs, we focused on two known maternal partners of Bcd: Hb which acts in synergy with Bcd (Porcher et al., 2010; Simpson-Brose et al., 1994) and Zld, the major regulator of early zygotic transcription in fruit fly (Liang et al., 2008). Interestingly, adding Zld or Hb sites next to the Bcd BS array reduces the time for the pattern to reach steady state and modify the promoter activity in different ways: binding of Zld facilitates the recruitment of Bcd at low concentration, making transcription more sensitive to Bcd and initiate faster while the binding of Hb affects strongly both the activation/deactivation kinetics of transcription and the RNAP firing rate. Thus, these two partners of Bcd contribute differently to Bcd-dependent transcription. Consistent with an activation process in two steps as proposed in our model, Zld will contribute to the first step favoring the precise and rapid measurements of positional information by Bcd without bringing itself positional information. Meanwhile, Hb will mostly act through the second step by increasing the level of transcription through a reduction of its burstiness and an increase in the polymerase firing rate. Interestingly, both Hb and Zld binding to the Bcd-dependent promoter allow speeding-up the establishment of the boundary, a property that Bcd alone is not able to achieve. Of note, the hb-P2 and Z2B6 reporters contain the same number of BS for Bcd and Zld but they have also very different boundary positions and mean onset time of transcription T_0 following mitosis when Bcd is limiting. This is likely due to the fact that the two Zld BS in the hb-P2 promoter of *hb* are not fully functional: one of the Zld BS is a weak BS while the other Zld BS has the sequence of a strong BS but is located too close from the TATA Box (5 bp) to provide full activity (Ling et al., 2019).

Zld functions as a pioneer factor by potentiating chromatin accessibility, transcription factor binding and gene expression of the targeted promoter (Foo et al., 2014; Harrison et al., 2011). Zld has recently been shown to bind nucleosomal DNA (McDaniel et al., 2019) and proposed to help establish or maintain cis-regulatory sequences in an open chromatin state ready for transcriptional activation (Eck

et al., 2020; Hannon et al., 2017). In addition, Zld is distributed in nuclear hubs or microenvironments of high concentration (Dufourt et al., 2018; Mir et al., 2018). Interestingly, Bcd has been shown to be also distributed in hubs even at low concentration in the posterior of the embryo (Mir et al., 2017). These Bcd hubs are Zld-dependent (Mir et al., 2017) and harbor a high fraction of slow moving Bcd molecules, presumably bound to DNA (Mir et al., 2018). Both properties of Zld, binding to nucleosomal DNA and/or the capacity to form hubs with increased local concentration of TFs can contribute to reducing the time required for the promoter to be occupied by a sufficient number of Bcd molecules for activation. In contrast to Zld, our knowledge on the mechanistic properties of the Hb protein in the transcription activation process is much more elusive. Hb synergizes with Bcd in the early embryo (Simpson-Brose et al., 1994) and the two TF contribute differently to the response with Bcd providing positional and Hb temporal information to the system (Porcher et al., 2010). Hb also contributes to the determination of neuronal identity later during development (Hirono et al., 2017). Interestingly, Hb is one of the first expressed members of a cascade of temporal TFs essential to determine the temporal identity of embryonic neurons in neural stem cells (neuroblasts) of the ventral nerve cord. In this system, the diversity of neuronal cell-types is determined by the combined activity of TFs specifying the temporal identity of the neuron and spatial patterning TFs, often homeotic proteins, specifying its segmental identity. How spatial and temporal transcription factors mechanistically cooperate for the expression of their target genes in this system is not known. Our work indicates that Hb is not able to activate transcription on its own but that it strongly increases RNAP firing probability and burst length of a locus licensed to be ON. Whether this capacity will be used in the ventral nerve cord and shared with other temporal TFs would be interesting to investigate.

The Bcd-only synthetic reporters also provided an opportunity to scrutinize the effect of Bcd concentration on the positioning of the expression domains. This question has been so far difficult to investigate with endogenous *hb* and hb-P2 reporters due to the presence of other TF BS in the promoter region which might mediate indirect effects of Bcd or Bcd-independent effects. When comparing the transcription patterns of the B9 reporter in Bcd-2X flies and Bcd-1X flies, we detected a shift of ~10.5 ± 1 %EL of the boundary position. Surprisingly, this shift revealed a gradient of Bcd activity with an exponential decay length of ~15 ± 1.4 %EL (~75 µm), significantly smaller than the value observed directly (~100 µm) with fluorescent-tagging (Gregor et al., 2007b; Liu et al., 2013) or immunofluorescence (Durrieu et al., 2018; Houchmandzadeh et al., 2002) of Bcd proteins. Importantly, reducing the decay length of the gradient also allows our model to fit significantly better the data. We propose that this decay length corresponds to a sub-population of "active" or "effective" Bcd distributed in a much steeper gradient than the Bcd gradient observed using immunofluorescence or GFP tagging which include all Bcd molecules. Bcd molecules have been shown to be heterogenous in intranuclear motility, age and spatial distributions but to date, we do not know which population of Bcd can access the target gene and activate transcription (Tran et al., 2020). The existence of two (or more) Bicoid populations with different mobilities (Abu-Arish et al., 2010; Fradin, 2017; Mir et al., 2018) obviously raises the question of the underlying gradient for each of them. Also, the dense Bcd hubs persist even in the posterior region where the Bcd concentration is low (Mir et al., 2017). As the total Bcd concentration decreases along the AP axis, these hubs accumulate Bcd with increasing proportion in the posterior, resulting in a steeper gradient of free-diffusing Bcd molecules outside the hubs. At last, the gradient of newly translated Bcd was also found to be steeper than the global gradient (Durrieu et al., 2018). Our work calls for further experiments to better characterize the roles of the different Bcd subpopulations. Importantly, reducing by half the Bcd concentration in the embryo induced a similar shift in the position of the hb-P2 reporter boundary as that of the Bcd-only reporters. This further argues that the effective gradient of Bcd activity, with a decay length λ_{eff} ~15 %EL, is a principal and direct source of positional information for *hb* expression.

The steeper effective Bcd gradient found here rekindles the debate on how a steep *hb* pattern can be formed in the early nuclear cycles. With the previous value of Bcd gradient decay length of λ =20 %EL, the Hill coefficient inferred from the fraction of loci's active time at steady state P_{Spot} is ~6.9, beyond the theoretical limit of the equilibrium model of Bcd interacting with 6 target BS of the *hb* promoter

(Estrada et al., 2016; Hopfield, 1974). This led to hypotheses of energy expenditure in Bcd binding and unbinding to the sites to overcome this limit (Estrada et al., 2016), *hb* promoters containing more than 6 Bcd sites (Lucas et al., 2018; Park et al., 2019) or additional sources of positional information (Tran et al., 2018). The effective decay length λ_{eff} ~15% EL, found here with a Bcd-only reporter but also hb-P2, corresponds to a Hill coefficient of ~5.2, just below the physical limit of an equilibrium model of concentration sensing with 6 Bcd BS alone. However, a smaller decay length also means that the effective Bcd concentration decreases faster along the AP axis. In the Berg & Purcell limit (Berg and Purcell, 1977), the time length to achieve the measurement error of 10% at hb-P2 expression boundary with λ=15 %EL is ~2.1 times longer than with λ=20 %EL (see Materials & Methods section H where we show the same argument holds regardless of estimated parameter values). This points again to the trade-off between reproducibility and steepness of the *hb* expression pattern, as described in (Tran et al., 2018).

Acknowledgement

We thank A. Coulon, A. Ramaekers, A. Taddei and the members of the Nuclear Dynamics Unit for fruitful discussions. We are indebted to BestGene Inc for transgenics and genome edition and to Patricia Le Baccon and the Imaging Facility PICT-IBiSA of the Institut Curie. This work is supported by PSL IDEX REFLEX Grant for Mesoscopic Biology (ND, AMW, MC), ANR-19-CE13-0025 FIREFLY (ND, AMW, CF), ARC PJA20151203341 (ND) and ANR-11-LABX-0044 DEEP Labex (ND, HT), Marie Skłodowska-Curie grant agreement No 666003 (GF), ARC DOC42021020003330 (GF) and NSERC discovery grant RGPIN-2015-06362 (CF, CPR). The funders had no role in study design, data collection and analysis, decision to publish, or preparation of the manuscript.

Reference

Abu-Arish, A., Porcher, A., Czerwonka, A., Dostatni, N., Fradin, C., 2010. High mobility of Bicoid captured by fluorescence correlation spectroscopy: Implication for the rapid establishment of its gradient. Biophys. J. 99, 33–35. https://doi.org/10.1016/j.bpj.2010.05.031

Berg, H.C., Purcell, E.M., 1977. Physics of chemoreception. Biophys. J. 20, 193–219. https://doi.org/10.1016/S0006-3495(77)85544-6

Bothma, J.P., Garcia, H.G., Esposito, E., Schlissel, G., Gregor, T., Levine, M., 2014. Dynamic regulation of eve stripe 2 expression reveals transcriptional bursts in living Drosophila embryos. Proc. Natl. Acad. Sci. 111, 10598–10603. https://doi.org/10.1073/pnas.1410022111

Crauk, O., Dostatni, N., 2005. Bicoid determines sharp and precise target gene expression in the Drosophila embryo. Curr. Biol. 15, 1888–1898. https://doi.org/10.1016/j.cub.2005.09.046

Desponds, J., Tran, H., Ferraro, T., Lucas, T., Perez Romero, C., Guillou, A., Fradin, C., Coppey, M., Dostatni, N., Walczak, A.M., 2016. Precision of readout at the hunchback gene: analyzing short transcription time traces in living fly embryos. PLOS Comput. Biol. 12, e1005256. https://doi.org/10.1371/journal.pcbi.1005256

Driever, W., Nusslein-Volhard, C., 1988. The Bicoid protein determines position in the Drosophila embryo in a concentration-dependent manner. Cell 54, 95–104. https://doi.org/10.1016/0092-8674(88)90183-3

Driever, W., Thoma, G., Nüsslein-Volhard, C., 1989. Determination of spatial domains of zygotic gene expression in the Drosophila embryo by the affinity of binding sites for the bicoid morphogen. Nature 340, 363–367. https://doi.org/10.1038/340363a0

Dufourt, J., Trullo, A., Hunter, J., Fernandez, C., Lazaro, J., Dejean, M., Morales, L., Nait-amer, S., Schulz, K.N., Harrison, M.M., Favard, C., Radulescu, O., Lagha, M., 2018. Temporal control of gene expression by the pioneer factor Zelda through transient interactions in hubs. Nat. Commun. 9, 1–13. https://doi.org/10.1038/s41467-018-07613-z

Durrieu, L., Kirrmaier, D., Schneidt, T., Kats, I., Raghavan, S., Hufnagel, L., Saunders, T.E., Knop, M., 2018. Bicoid gradient formation mechanism and dynamics revealed by protein lifetime analysis. Mol. Syst. Biol. 14, e8355. https://doi.org/10.15252/msb.20188355

Eck, E., Liu, J., Kazemzadeh-Atoufi, M., Ghoreishi, S., Blythe, S., Garcia, H., 2020. Quantitative dissection of transcription in development yields evidence for transcription factor-driven chromatin accessibility. eLife. https://doi.org/10.1101/2020.01.27.922054

Estrada, J., Wong, F., DePace, A., Gunawardena, J., 2016. Information integration and energy expenditure in gene regulation. Cell 166, 234–244. https://doi.org/10.1016/j.cell.2016.06.012

Ferraro, T., Lucas, T., Clémot, M., De Las Heras Chanes, J., Desponds, J., Coppey, M., Walczak, A.M., Dostatni, N., 2016. New methods to image transcription in living fly embryos: The insights so far, and the prospects. Wiley Interdiscip. Rev. Dev. Biol. 5, 296–310. https://doi.org/10.1002/wdev.221

Foo, S.M., Sun, Y., Lim, B., Ziukaite, R., O'Brien, K., Nien, C.-Y., Kirov, N., Shvartsman, S.Y., Rushlow, C.A., 2014. Zelda potentiates morphogen activity by increasing chromatin accessibility. Curr. Biol. CB 24, 1341–1346. https://doi.org/10.1016/j.cub.2014.04.032

Fradin, C., 2017. On the importance of protein diffusion in biological systems: The example of the Bicoid morphogen gradient. Biochim. Biophys. Acta - Proteins Proteomics 1865, 1676–1686. https://doi.org/10.1016/j.bbapap.2017.09.002

Fukaya, T., Lim, B., Levine, M., 2017. Rapid rates of Pol II elongation in the Drosophila embryo. Curr. Biol. 27, 1387–1391. https://doi.org/10.1016/j.cub.2017.03.069

Garcia, H.G., Tikhonov, M., Lin, A., Gregor, T., 2013. Quantitative imaging of transcription in living Drosophila embryos links polymerase activity to patterning. Curr. Biol. 23, 2140–2145. https://doi.org/10.1016/j.cub.2013.08.054

Gratz, S.J., Rubinstein, C.D., Harrison, M.M., Wildonger, J., O'Connor-Giles, K.M., 2015. CRISPR-Cas9 Genome Editing in Drosophila. Curr. Protoc. Mol. Biol. 111, 31.2.1-31.2.20. https://doi.org/10.1002/0471142727.mb3102s111

Gregor, T., Tank, D.W., Wieschaus, E., Bialek, W., 2007a. Probing the limits to positional information. Cell 130, 153–164. https://doi.org/10.1016/j.cell.2007.05.025

Gregor, T., Wieschaus, E., McGregor, A.P., Bialek, W., Tank, D.W., 2007b. Stability and nuclear dynamics of the Bicoid morphogen gradient. Cell 130, 141–152. https://doi.org/10.1016/j.cell.2007.05.026

Hanes, S.D., Brent, R., 1989. DNA specificity of the bicoid activator protein is determined by homeodomain recognition helix residue 9. Cell 57, 1275–1283. https://doi.org/10.1016/0092-8674(89)90063-9

Hannon, C.E., Blythe, S.A., Wieschaus, E.F., 2017. Concentration dependent chromatin states induced by the bicoid morphogen gradient. eLife 6:e28275, 1–29. https://doi.org/10.7554/eLife.28275

Harrison, M.M., Li, X.Y., Kaplan, T., Botchan, M.R., Eisen, M.B., 2011. Zelda binding in the early Drosophila melanogaster embryo marks regions subsequently activated at the maternal-to-zygotic transition. PLoS Genet. 7. https://doi.org/10.1371/journal.pgen.1002266

Hirono, K., Kohwi, M., Clark, M.Q., Heckscher, E.S., Doe, C.Q., 2017. The Hunchback temporal transcription factor establishes, but is not required to maintain, early-born neuronal identity. Neural Develop. 12. https://doi.org/10.1186/s13064-017-0078-1

Hopfield, J.J., 1974. Kinetic proofreading: A new mechanism for reducing errors in biosynthetic processes requiring high specificity. Proc. Natl. Acad. Sci. U. S. A. 71, 4135–4139. https://doi.org/10.1073/pnas.71.10.4135

Houchmandzadeh, B., Wieschaus, E., Leibler, S., 2002. Establishment of developmental precision and proportions in the early Drosophila embryo. Nature 415, 798–802. https://doi.org/10.1038/415798a

Lagarias, J.C., Reeds, J.A., Wright, M.H., Wright, P.E., 1998. Convergence properties of the Nelder-Mead simplex method in low dimensions. SIAM J. Optim. 9, 112–147. https://doi.org/10.1137/S1052623496303470

Lammers, N.C., Galstyan, V., Reimer, A., Medin, S.A., Wiggins, C.H., Garcia, H.G., 2019. Multimodal transcriptional control of pattern formation in embryonic development. Dev. Biol. https://doi.org/10.1101/335919

Liang, H.-L., Nien, C.-Y., Liu, H.-Y., Metzstein, M.M., Kirov, N., Rushlow, C., 2008. The zinc-finger protein Zelda is a key activator of the early zygotic genome in Drosophila. Nature 456, 400–403. https://doi.org/10.1038/nature07388

Ling, J., Umezawa, K.Y., Scott, T., Small, S., 2019. Bicoid-dependent activation of the target gene hunchback requires a two-motif sequence code in a specific basal promoter. Mol. Cell 1–10. https://doi.org/10.1016/j.molcel.2019.06.038

Little, S.C., Tikhonov, M., Gregor, T., 2013. Precise developmental gene expression arises from globally stochastic transcriptional activity. Cell 154, 789–800. https://doi.org/10.1016/j.surg.2006.10.010.Use

Liu, F., Morrison, A.H., Gregor, T., 2013. Dynamic interpretation of maternal inputs by the Drosophila segmentation gene network. Proc. Natl. Acad. Sci. 110, 6724–6729. https://doi.org/10.1073/pnas.1220912110

Lopes, F.J., Spirov, A.V., Bisch, P.M., 2011. The role of Bicoid cooperative binding in the patterning of sharp borders in Drosophila melanogaster. Dev. Biol. 72, 181–204. https://doi.org/10.1038/nature13314.A

Lucas, T., Tran, H., Romero, C.A.P., Guillou, A., Fradin, C., Coppey, M., Walczak, A.M., Dostatni, N., 2018. 3 Minutes To precisely measure morphogen concentration. PLoS Genet. 14, e1007676. https://doi.org/10.1101/305516

McDaniel, S.L., Gibson, T.J., Schulz, K.N., Fernandez Garcia, M., Nevil, M., Jain, S.U., Lewis, P.W., Zaret, K.S., Harrison, M.M., 2019. Continued activity of the pioneer factor Zelda is required to drive zygotic genome activation. Mol. Cell 74, 185-195.e4. https://doi.org/10.1016/j.molcel.2019.01.014

Mir, M., Reimer, A., Haines, J.E., Li, X.Y., Stadler, M., Garcia, H., Eisen, M.B., Darzacq, X., 2017. Dense bicoid hubs accentuate binding along the morphogen gradient. Genes Dev. 31, 1784–1794. https://doi.org/10.1101/gad.305078.117

Mir, M., Stadler, M.R., Harrison, M.M., Darzacq, X., Eisen, M.B., 2018. Dynamic multifactor hubs interact transiently with sites of active transcription in Drosophila embryos. eLife 7.

Park, J., Estrada, J., Johnson, G., Ricci-Tam, C., Bragdon, M.D., Shulgina, Y., Cha, A., Gunawardena, J., Depace, A.H., Vincent, B.J., Ricci-Tam, C., Bragdon, M.D., Shulgina, Y., Cha, A., Wunderlich, Z., Gunawardena, J., Depace, A.H., 2019. Dissecting the sharp response of a canonical developmental enhancer reveals multiple sources of cooperativity. eLife 8, 1–25. https://doi.org/10.7554/eLife.41266

Perez-Romero, C.A., Tran, H., Coppey, M., Walczak, A.M., Fradin, C., Dostatni, N., 2018. Live imaging of mRNA transcription in Drosophila embryos, in: Dubrulle, J. (Ed.), Methods in Molecular Biology - Morphogen Gradients. Springer, pp. 165–182. https://doi.org/10.1007/978-1-4939-8772-6_10

Petkova, M.D., Little, S.C., Liu, F., Gregor, T., 2014. Maternal origins of developmental reproducibility. Curr. Biol. 24, 1283–1288. https://doi.org/10.1016/j.cub.2014.04.028

Porcher, A., Abu-Arish, A., Huart, S., Roelens, B., Fradin, C., Dostatni, N., 2010. The time to measure positional information: maternal hunchback is required for the synchrony of the Bicoid transcriptional response at the onset of zygotic transcription. Development 137, 2795–804. https://doi.org/10.1242/dev.051300

Port, F., Chen, H.-M., Lee, T., Bullock, S.L., 2014. Optimized CRISPR/Cas tools for efficient germline and somatic genome engineering in Drosophila. Proc. Natl. Acad. Sci. 111, E2967–E2976. https://doi.org/10.1073/pnas.1405500111

Simpson-Brose, M., Treisman, J., Desplan, C., 1994. Synergy between the hunchback and bicoid morphogens is required for anterior patterning in Drosophila. Cell 78, 855–865. https://doi.org/10.1016/S0092-8674(94)90622-X

Struhl, G., Struhl, K., Macdonald, P.M., 1989. The gradient morphogen bicoid is a concentration-dependent transcriptional activator. Cell 57, 1259–1273. https://doi.org/10.1016/0092-8674(89)90062-7

Tran, H., Desponds, J., Romero, C.A.P., Coppey, M., Fradin, C., Dostatni, N., Walczak, A.M., 2018a. Precision in a rush: trade-offs between reproducibility and steepness of the hunchback expression pattern. PLoS Comput. Biol. 14, e1006513. https://doi.org/. https://doi.org/10.1371/journal. pcbi.1006513

Tran, H., Perez-Romero, C.A., Ferraro, T., Fradin, C., Dostatni, N., Coppey, M., Walczak, A.M., 2018b. LiveFly: A toolbox for the analysis of Transcription Dynamics in live Drosophila embryos, in: Dubrulle, J. (Ed.), Methods in Molecular Biology - Morphogen Gradients. Springer, pp. 183–195. https://doi.org/10.1007/978-1-4939-8772-6_11

Tran, H., Walczak, A.M., Dostatni, N., 2020. Constraints and limitations on the transcriptional response downstream of the Bicoid morphogen gradient, in: Current Topics in Developmental Biology - Gradients and Tissue Patterning. pp. 119–142. https://doi.org/10.1101/728840

Treisman, J., Gönczy, P., Vashishtha, M., Harris, E., Desplan, C., 1989. A single amino acid can determine the DNA binding specificity of homeodomain proteins. Cell 59, 553–562. https://doi.org/10.1016/0092-8674(89)90038-x

Venken, K.J.T., He, Y., Hoskins, R.A., Bellen, H.J., 2006. P[acman]: A BAC Transgenic Platform for targeted insertion of large DNA fragments in D. melanogaster. Science 314, 1747–1751. https://doi.org/10.1126/science.1134426

Xu, Z., Chen, H., Ling, J., Yu, D., Struffi, P., Small, S., 2014. Impacts of the ubiquitous factor Zelda on Bicoid-dependent DNA binding and transcription in Drosophila. Genes Dev. 28, 608–621. https://doi.org/10.1101/gad.234534.113

Figure 1

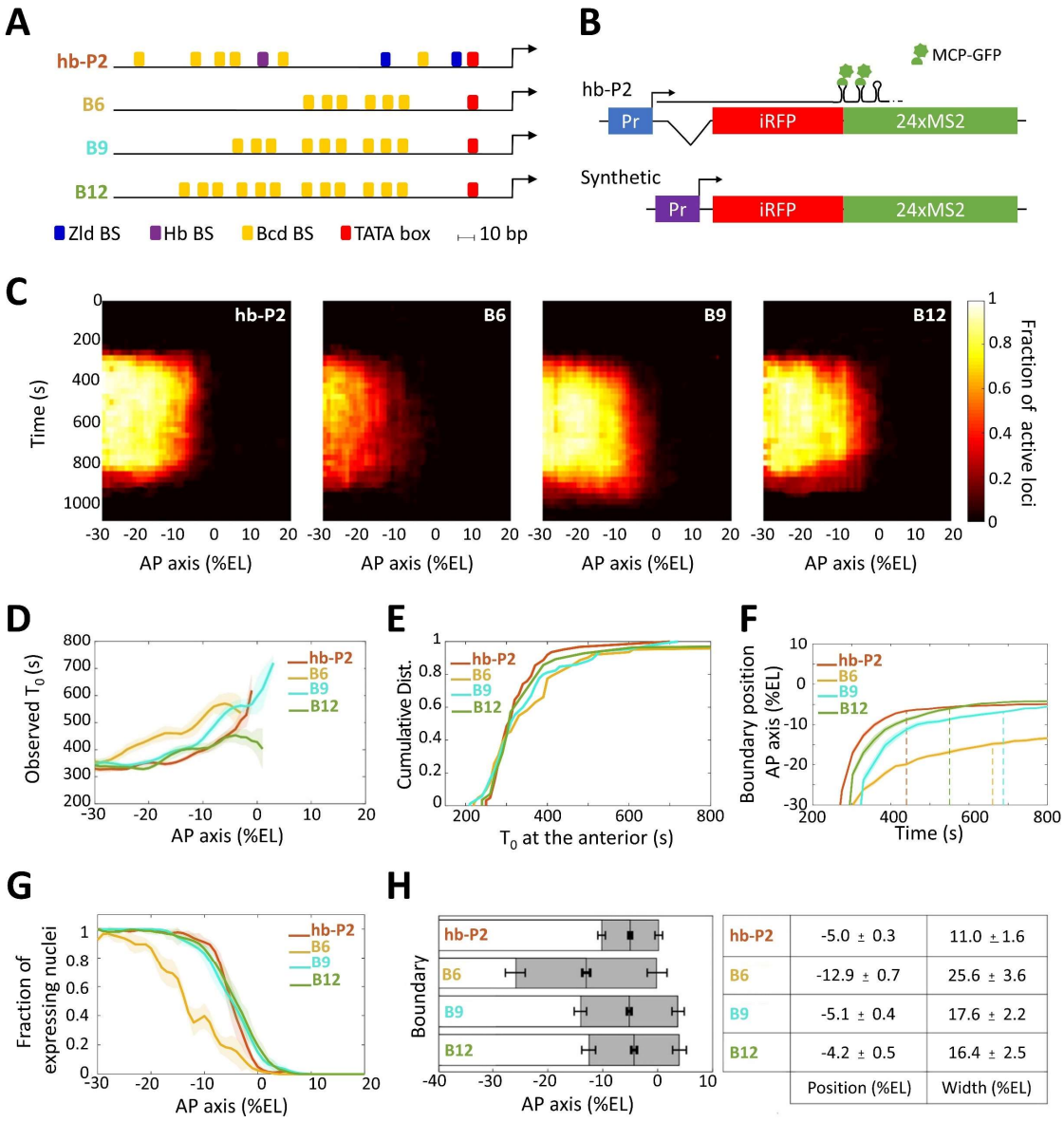

Figure 1. Transcription dynamics of the hb-P2, B6, B9 and B12 reporters

A) Arrangement of the binding sites for Bcd (yellow), Hb (purple) and Zld (blue) upstream of the TATA box (red) and the TSS (broken arrow) of each reporter. **B**) The MS2 reporters express the iRFP coding sequence followed by the sequence of the 24 MS2 stem loops. In the hb-P2 reporter, the hb-P2 promoter, 5'UTR sequence of the endogenous *hb* and its intron are placed just upstream of the iRFP sequence. In the synthetic reporters, the minimal promoter of the hsp70 gene was used. Of note, replacing the minimal promoter of hsp70 in B6 by the *hb* minimal promoter leads to a reporter with lower activity (Fig. S1, F-G). **C**) Kymographs of mean fraction of active loci (colormap on the right) as a function of time (Y axis in s) and nuclei position along the AP axis (X axis in %EL) at nc13. **D**) Along the AP axis (%EL), mean time of first spot appearance T_0 (s) with shaded standard error of the mean and calculated only for loci with observed expression. **E**) Cumulative distribution function of T_0 (s) in the anterior (-30 ± 2.5 %EL). **F**) Boundary position (%EL) of fraction of nuclei with MS2 signal along AP axis, with shaded 95% confidence interval, as a function of time. The dash vertical lines represent the time to reach the final decision boundary position (±2 %EL). **G**) Fraction of nuclei with any MS2 signal, averaged over n embryos, with shaded standard error of the mean, along the AP axis (%EL), at nc13. **H**) Boundary position and width were extracted by fitting the patterns (fraction of expressing nuclei,

G) with a sigmoid function. Bar plots with 95% confidence interval for boundary position and width as the grey region placed symmetrically around the boundary position. Average values and confidence intervals are indicated in the adjacent table. **D-H**) reporter data are distinguished by color: hb-P2 (orange, n=5 embryos), B6 (yellow, n=5 embryos), B9 (cyan, n=6 embryos) and B12 (green, n=4 embryos).

Figure 2

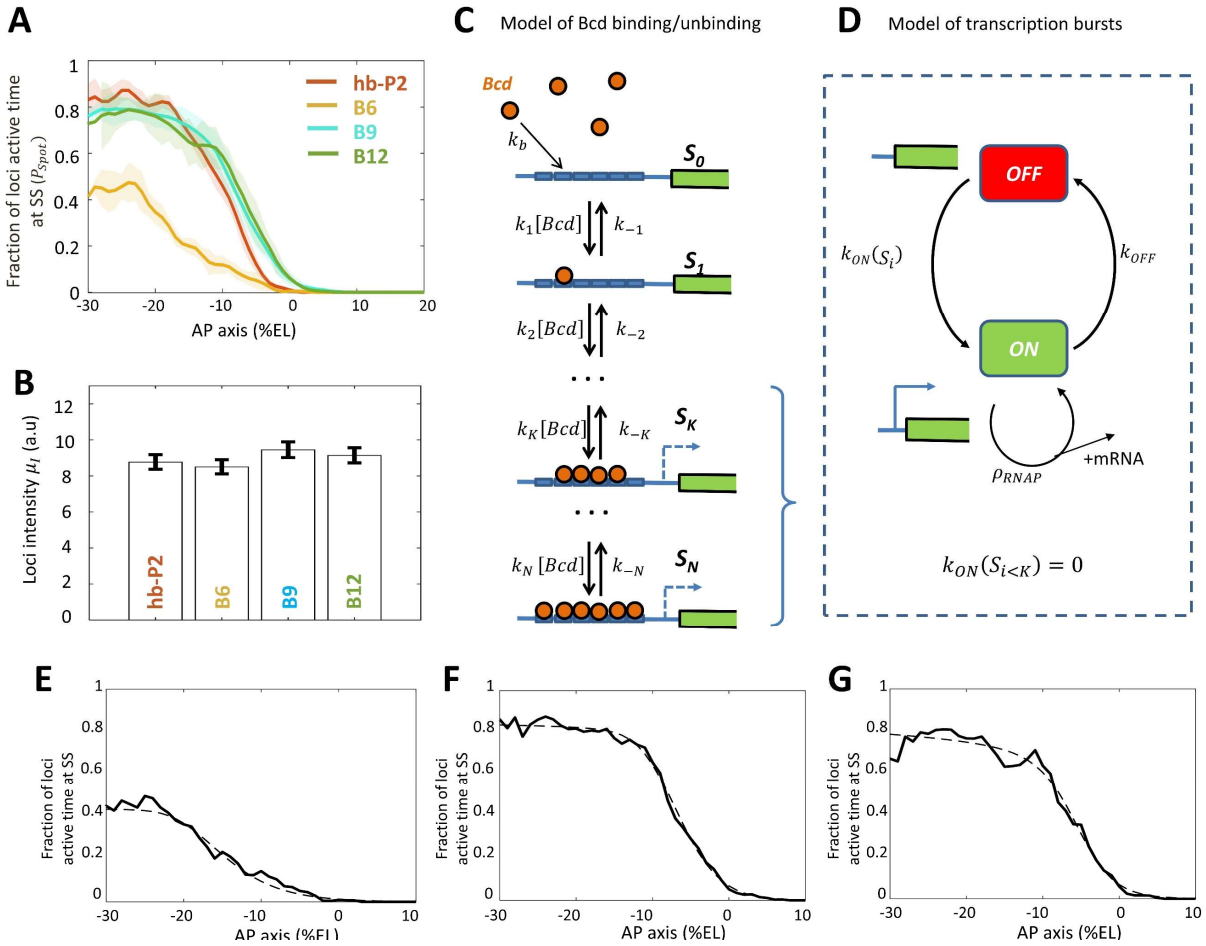

Figure 2. Modeling transcription dynamics at steady state.

A) Fraction of loci active time (P_{Spot}) at steady state (time window of 600 - 800 s into nc13), averaged over n embryos, as a function of nuclei position along AP axis (%EL). **B**) Mean fluorescent intensity (μ_I) with standard error of active MS2 loci detected in the anterior region (~ -30% EL) at steady state. In A-B) reporter data are distinguished by color: hb-P2 (orange, n=5 embryos), B6 (yellow, n=5 embryos), B9 (cyan, n=6 embryos) and B12 (green, n=4 embryos). **C**) Model of Bicoid binding and unbinding to an array of N identical binding sites: nuclear Bcd molecules can bind independently to individual binding sites at rate k_b. The binding array state is denoted by S_i where i is the number of bound sites. The forward rate constants k_i are the binding rates of Bcd to the free remaining sites of S_{i-1}: $k_i = (N - i + 1)k_b$. The backward rate constants k_{-i} are the unbinding rates of bound Bcd from S_i. **D**) Transcription dynamics is modeled as a bursty two-state ON/OFF model with the switching rate constants $k_{ON}(S_i)$ and k_{OFF}. The switching rate $k_{ON}(S_i)$ depends on i the number of bound Bcd molecules. Transcription is not activated with fewer than K bound Bcd ($k_{ON}(S_{i<K}) = 0$). Only during the ON state can RNAPs arrive and initiate transcription at rate constant ρ_{RNAP}. **E-G**) Fit of B6 (panel E), B9 (panel F), B12 (panel G) patterns at steady state with models of corresponding BS numbers (N=6 for B6, N=9 for B9, N=12 for B12). In these models, the free parameters are the unbinding rate constant (k_{-i}), the promoter switching rates with K bound Bcd molecules ($k_{ON}(S_K)$ and k_{OFF}). K is

set to 3. The switching ON rates at higher bound states are set $k_{ON}(S_{i>K}) = k_{ON}(S_K)[\frac{i}{K}]$, given the synergistic activation of transcription by bound Bcd (see Material & Method section G). The binding rate constant k_b is determined by assuming that Bcd binding is diffusion limited (Material & Method section F). Shown are the transcription patterns from the data (solid) and the predicted patterns from the fitted model (dashed).

Figure 3

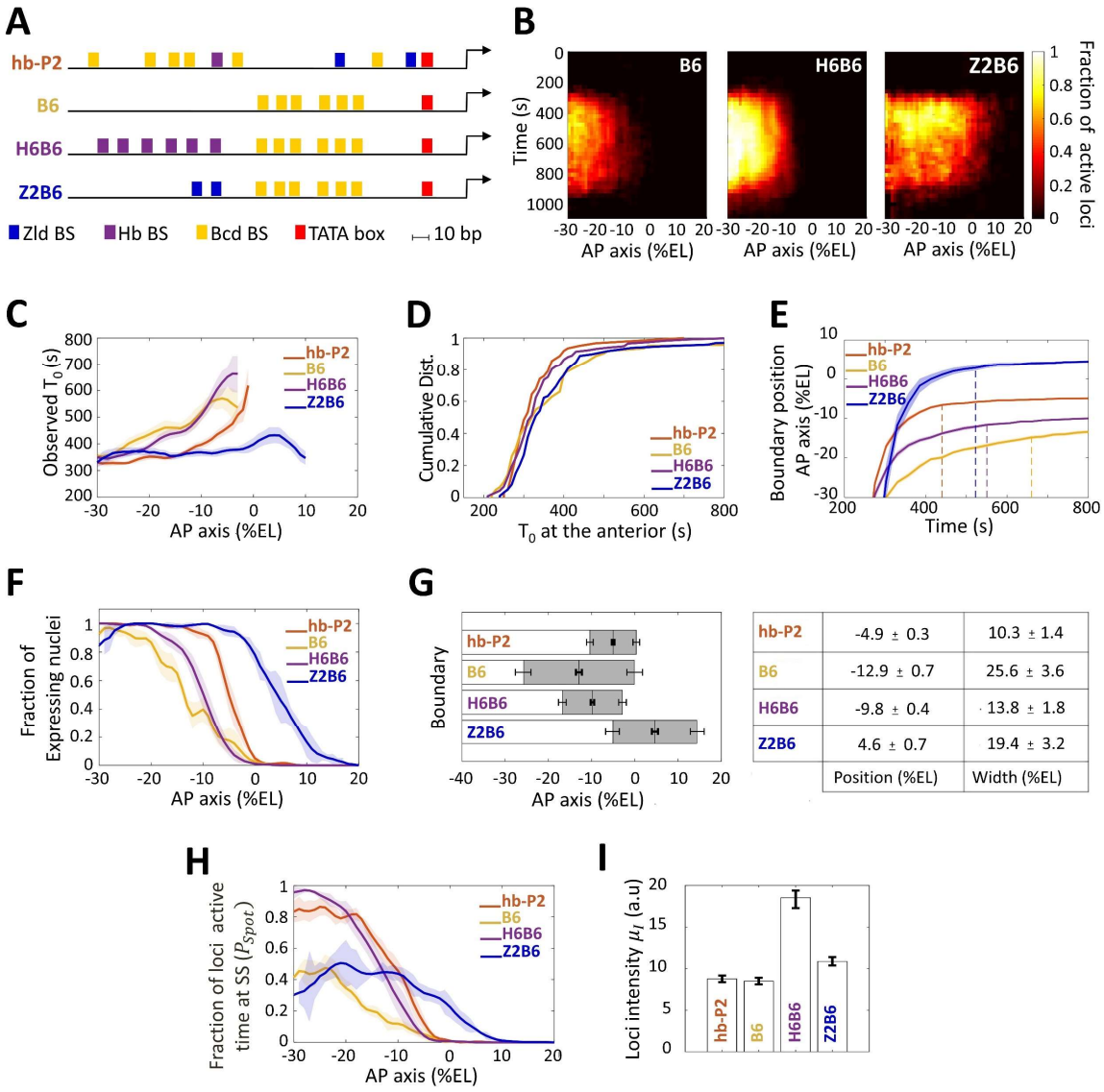

Figure 3. Transcription dynamics of the B6, H6B6 and Z2B6 reporters

A) Arrangement of the binding sites for Bcd (yellow), Hb (purple) and Zld (blue) upstream of the TATA box (red) and the TSS (broken arrow) of each reporter. **B**) Kymographs of mean fraction of active loci (colormap on the right) as a function of time (Y axis in s) and nuclei position along the AP axis (X axis in %EL) at nc13. **C**) Mean time of first spot appearance T_0 (s) along the AP axis with shaded standard error of the mean and calculated only for loci with observed expression. **D**) Cumulative distribution function of T_0 (s) at the anterior (-30 ± 2.5 %EL). **E**) Boundary position (as %EL) of fraction of nuclei with MS2 signal along AP axis, with shaded 95% confidence interval, as a function of time. The dash vertical curves represent the time to reach the final decision boundary position (±2 %EL). **F**) Fraction of nuclei with any MS2 signal along the AP axis (%EL) with shaded standard error of the mean. **G**) Boundary position and width were extracted by fitting the patterns (fraction of expressing nuclei, F) with a

sigmoid function. Bar plots with 95% confidence interval for boundary position and width as the grey region placed symmetrically around the boundary position. Average values and confidence intervals are indicated in the adjacent table. **H**) Fraction of loci active time (P_{Spot}) at steady state (time window of 600 - 800 s into nc13) as a function of nuclei position along AP axis. **I**) Mean intensity (μ_I) with standard error of active fluorescent loci detected in the anterior region (~-30% EL) at steady state. **C-I**) reporter data are distinguished by color: hb-P2 (orange, n=5 embryos), B6 (yellow, n=5 embryos), H6B6 (purple, n=7 embryos) and Z2B6 (blue, n=3 embryos).

Figure 4

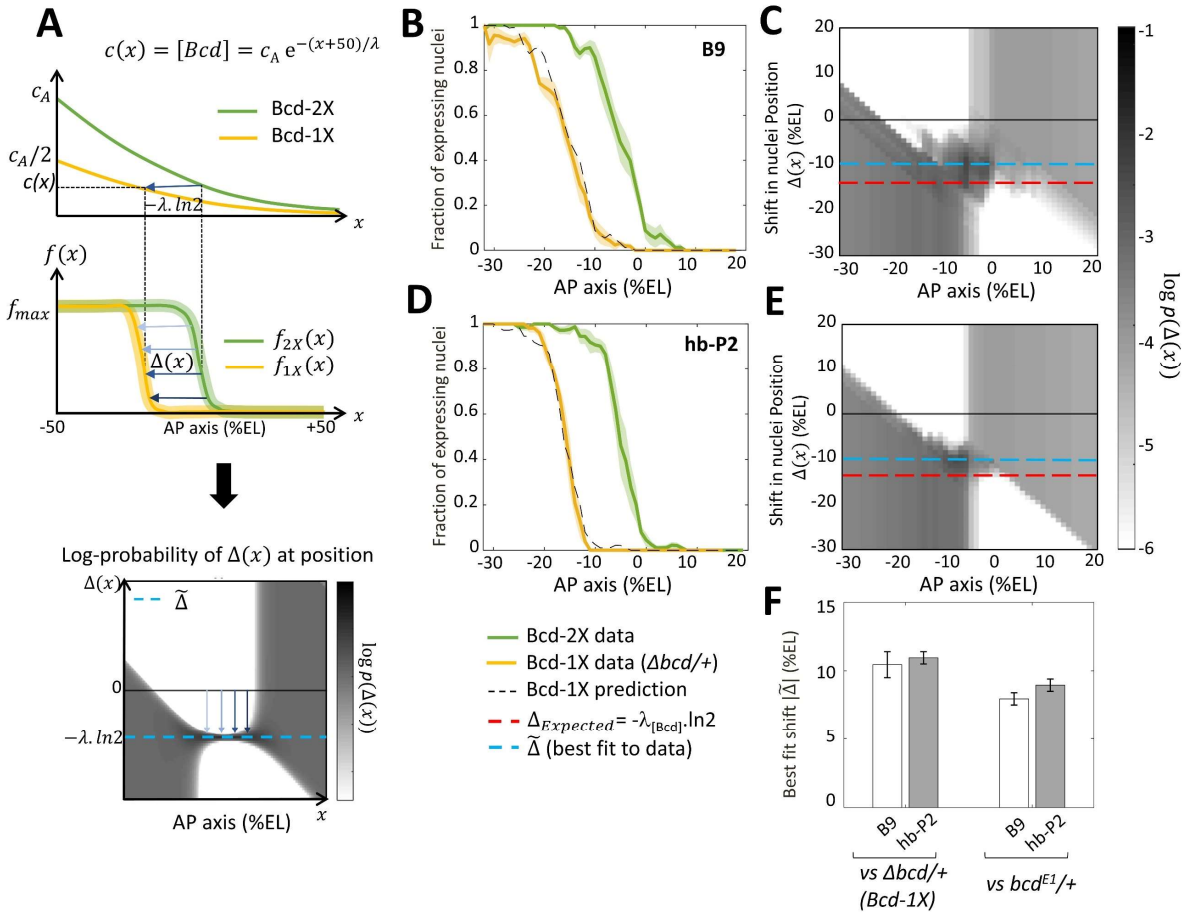

Figure 4. Bicoid thresholds measurements by the Bcd-only synthetic reporters

A) Modeling the pattern shifts between Bcd-2X and Bcd-1X embryos. Top: The Bcd concentration gradient along the AP axis with its exponential decay length λ. At the anterior pole, Bcd concentration is c_A in Bcd-2X embryos (solid green line) and $c_A/2$ in Bcd-1X embryos (solid yellow line). The distance between any two nuclei columns in Bcd-2X and Bcd-1X that have the same Bcd concentration (blue arrow) is given by $-\lambda\, ln2$. Middle: along the AP axis, expression pattern of a Bcd-dependent reporter in Bcd-2X embryos ($f_{2X}(x)$, solid green line) and in Bcd-1X embryos ($f_{1X}(x)$solid yellow line). $\Delta(x)$: the shift in position (blue directed arrows) from a nuclei column in Bcd-2X embryos at position x to one at Bcd-1X embryos with the same expression level, such that $f_{2X}(x) = f_{1X}(x - \Delta(x))$. Bottom: Cartoon of log-probability map of the shift $\Delta(x)$ based on the expression patterns in Bcd-2X and Bcd-1X (i.e. *f*). Its value $\log p(\Delta(x))$ is represented on the grey scale. The blue directed arrows denoting the shift correspond to arrows with similar shade observed in the bottom left panel. If the Bcd gradient is the only source of positional information for the expression patterns, then the best fit value of $\Delta(x)$ given the probability map is $\tilde{\Delta} = -\lambda ln2$ (horizontal blue dashed line). **B** & **D**) Expression patterns of B9 (panel B) and hb-P2 (panel D) reporters in embryos from wild-type (Bcd-2X, solid green lines with

shaded errors) and Δ*bcd*/+ (Bcd-1X, solid yellow lines with shaded errors) females. Prediction of Bcd-1X pattern from the Bcd-2X pattern assuming a fitted constant shift $\widetilde{\Delta}$ = 10.5±1.0 %EL for B9 and $\widetilde{\Delta}$ = 11.0±0.5 %EL for hb-P2 (black dashed line). For B9 (B) data were from n_{2x} = 6 embryos and n_{1x} = 6 embryos and for hb-P2, data were from n_{2x} = 5 embryos and n_{1x}= 3 embryos. **C** & **E**) Log-probability map ($\log p(\Delta(x))$ of the shift $\Delta(x)$ (in %EL) at a given nuclei position in Bcd-2X embryos (x, in %EL), extracted from the experimental data. The horizontal cyan dashed line represents $\widetilde{\Delta}$ the best fit value of $\widetilde{\Delta}$ for B9 (panel C) and for hb-P2 (panel E). The horizontal red dashed line represents the expected shift $\Delta_{Expected}$= -$\lambda_{[Bcd]} ln2$ given $\lambda_{[Bcd]}$=20 %EL the detected decay length of the Bcd gradient (Gregor et al., 2007b; Houchmandzadeh et al., 2002). **F**) Comparison of the fitted shift, with 95% confidence interval, in nuclei position from wild-type embryos to embryos from Δ*bcd*/+ females (left bars) and from wild-type embryos to embryos from bcd^{E1}/+ females (right bars) with B9 and hb-P2 reporters.

Figure 5

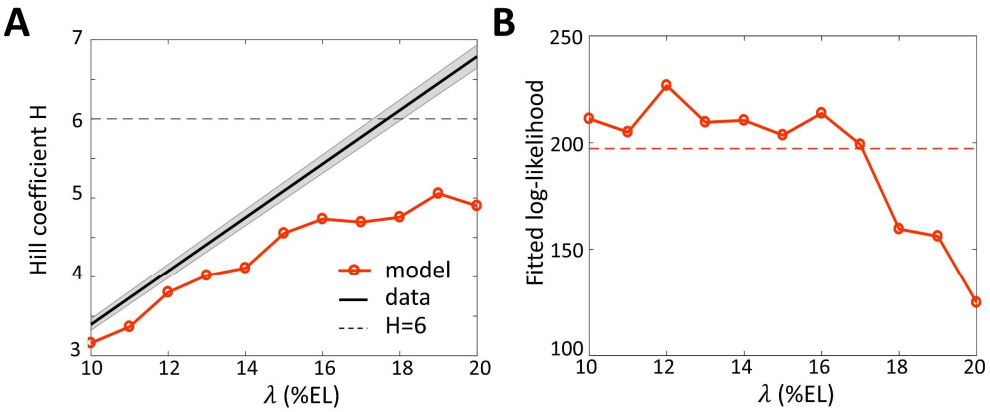

Figure 5: Fitting the data with models assuming different values for the Bcd gradient decay length λ. A) Hill coefficient H (see Material & Methods section C) (solid red) in the steady state window (600s-800s into nc13 interphase) calculated numerically from the best fitted models. Given that the pattern sharpness $\eta = H/\lambda$ is measured to be 0.34 from the hb-P2 data, the observed Hill coefficient as a function of λ is given by the black line with shaded error. The physical limit of equilibrium sensing model with 6 BS (H = 6, black dashed line). B) Log-likelihood of the best fitted models (solid red). The dashed line corresponds to the log-likelihood thresholds for a significantly worse fit (p-value=0.05).

MATERIAL AND METHODS

RESOURCE AVAILABILITY

Further information and requests for raw data, resources and reagents should be directed to and will be fulfilled by the lead contact, Nathalie Dostatni (Nathalie.Dostatni@curie.fr).

EXPERIMENTAL MODEL AND SUBJECT DETAILS

Drosophila stocks

Embryos were obtained from crosses between females carrying the MCP-NoNLS-eGFP (Garcia et al., 2013) and the His2Av-mRFP (Bloomington # 23561) transgenes both on the second chromosome with males expressing MS2 reporters. Embryos with half dose of Bcd were obtained from females which were in addition heterozygotes for the bcd^{E1} amorphic allele (bcd^{6}). Unless otherwise specified, all MS2 reporters were inserted at the vk33 docking site (Bloomington # 9750) via ϕC31 mediated integration system (Venken et al., 2006) by BestGene. The site of insertion was chosen because the transcription dynamics of the original hb-P2 reporter (Lucas et al., 2018) inserted at this site was indistinguishable from the transcription dynamics of two randomly inserted siblings (Fig. S1A-C). All fly stocks were maintained at 25°C.

MS2 reporters

The hb-P2 MS2 reporter was obtained by cloning the 745bp (300bp upstream of the transcription start site to 445 bp downstream, including the hb intron) located just upstream start codon of Hunchback protein (*Drosophila melanogaster*) from the previously used hb-MS2ΔZelda reporter (Lucas et al., 2018) into the attB-P[acman]-Cm^{R}-BW plasmid. The synthetic MS2 reporters were created by replacing the *hb* region in hb-P2 MS2 by the *hsp70Bb* promoter and the synthetic sequences containing specific combinations of binding sites. GGGATTA was used as a Bcd binding site, CAGGTAG as a Zld binding site and TCAAAAAATAT or TCAAAAAACTAT as Hb binding sites. The sequences of these promoters are in the table S1.

Generation of the Δbcd mutant by CRISPR

The Δ*bcd* molecular null allele was generated by CRISPR/Cas9 genome editing using the scarless strategy described in (Gratz et al., 2015). gRNA sequences were designed to induce Cas-9 dependent double strand DNA hydrolysis 460 pb upstream of the *bcd* gene TATA box and 890 bp downstream of the Bcd stop codon. For this, double stranded oligonucleotides (sequences available in Table S1: Oligo for 5' cut Fw, Oligo for 5' cut Rv, Oligo for 3' cut Fw, Oligo for 3' cut Rv) were inserted into the Bbs-1 restriction site of pCFD3-dU6_3gRNA vector (Port et al., 2014). The two homology arms flanking the cleavage sites were amplified from genomic DNA by PCR using the NEB Q5 high fidelity enzyme and specific oligonucleotides (sequences available in Table S1: Bcdnull_5HR_fw, Bcdnull_5HR_rv, Bcdnull_3HR_fw, Bcdnull_3HR_rv). The scarless-DsRed sequence was amplified by with Q5 from the pHD-ScarlessDsRed vector using specific oligonucleotides (sequences available in Table S1: Bcdnull_DsRed_fw, Bcdnull_DsRed_rv). The three PCR amplified fragments were mixed in equimolar ratio with the 2835 bp SapI-AarI fragment of pHD-ScarlessDsRed for Gibson assembly using the NEBuilder system. Injections and recombinant selection based on DsRed expression in the eye were performed by BestGene. For transformants, sequences at the junctions between deletion break point and the inserted dsRed marker were amplified by PCR and verified by sequencing.

METHOD DETAILS

A. Live Embryo imaging

Sample preparation and live imaging of transcription was performed as in (Perez-Romero et al., 2018). Briefly, embryos were collected 30 minutes after egg laying, dechorionated by hand and mounted on coverslips covered in heptane-dissolved glue and immersed in 10S Voltatef oil (VWR). All embryos were imaged between nc10 and nc14 at stable temperature (25°C) on a LSM780 confocal microscope equipped with a 40x (1.4 NA Plan-Apochromat) oil immersion objective. For each embryo, a stack of images is acquired (0.197µm pixel size, 8 bit per pixel, 0.55µs pixel dwell time, confocal pinhole diameter of 92µm, 0.75µm distance between consecutive images in the stack, ~1200x400 pixels image size). GFP and RFP proteins were imaged with 488nm and 561nm lasers, respectively, with appropriate power output. Embryo size and position of the imaged portion is calculated through imaging and measurement of a tiled image of the sagittal plane of the embryo.

B. Data extraction

Data extraction from MS2 movies was performed as in (Lucas et al., 2018) using the LiveFly toolbox (Tran et al., 2018b). In brief, nuclei were segmented in a semi-automatic manner based on His2Av-mRFP channel. The active MS2 loci detection was performed in 3D using a thresholding method. The pixel values at the detected loci location were then fitted with a gaussian kernel to obtain the MS2 loci intensity. The expression data containing each nucleus' position along AP axis and MS2 loci intensity trace over time was exported.

From each time trace in individual nuclei in nc13, we extracted three features: the detection of MS2 expression during the nuclear interphase (taking 0 or 1 values), T_0 the time of first MS2 spot appearance and P_{Spot} the probability of detecting a spot during the steady state window. This window is defined to be 600-800s into nc13 due to a transient "surge" in transcription activity with the hb-P2 reporter inserted in the vk33 (Fig. S1).

C. Quantifying pattern sharpness, boundary width and Hill coefficient

To quantify the sharpness of the transcription patterns of *ms2* reporters, we fit the patterns along the AP axis to a sigmoid function:

$$f_{Sigmoid}(x) = f_{max}\frac{e^{-x\eta}}{e^{-x\eta}+e^{-x_0\eta}}. \quad (1)$$

In Eq. 1, x is the position of the nuclei. f_{max} is the maximum expression level at the anterior pole ($f_{max} = f_{Sigmoid}(x = -\infty)$). x_0 is the expression boundary position ($f_{Sigmoid}(x_0) = f_{max}/2$). η is the scaling coefficient of the AP axis. η also corresponds to the pattern sharpness as it is the derivative of the sigmoid function at the boundary position divided by f_{max}.

From the fitted pattern, we define the boundary width as the distance between two nuclei columns with $f_{Sigmoid}(x)$ of 5% and 95% of maximum expression level f_{max}.

$$\text{Boundary width} = 2\ln\left(\frac{0.95}{0.05}\right)/\eta = 5.59/\eta. \quad (2)$$

We assume an exponential Bcd gradient with the decay length λ ($[Bcd] = c_0 e^{-x/\lambda}$), where c_0 is Bcd concentration at x=0. We replace $x = -\lambda\log([Bcd]/c_0)$ and find the gene expression pattern from the promoter:

$$f_{regulation}([Bcd]) = f_{max}\frac{e^{-\lambda.\log([Bcd]/c_0)\eta}}{e^{-\lambda.\log([Bcd]/c_0)\eta} + e^{-x_0\eta}} = f_{max}\frac{\left(\frac{[Bcd]}{c_0}\right)^{\lambda\eta}}{\left(\frac{[Bcd]}{c_0}\right)^{\lambda\eta} + e^{-x_0\eta}} = f_{max}\frac{[Bcd]^{\lambda\eta}}{[Bcd]^{\lambda\eta} + c_0^{\lambda\eta}e^{-x_0\eta}}. \quad (3)$$

One should note that in Eq. 3 the Hill function with the Hill coefficient H depends on both the pattern sharpness η and the decay length of the Bcd gradient λ:

$$H = \lambda\eta. \quad (4)$$

In Eq. 4, the pattern sharpness η can be extracted directly from the ms2 movies. Therefore, the assumptions on the decay length λ will determine the inferred Hill coefficient H and consequently the requirements of Bcd binding cooperativity and energy expenditure to achieve such coefficients (Estrada et al., 2016; Tran et al., 2018a).

D. Simulating the model of transcription regulation by Bcd

For a model of transcription regulation with N Bcd binding sites, the system can be in 2xN+2 states, that consists of (N+1) binding array states (S_0 to S_N) and 2 transcriptional states (ON and OFF).

We define the state probability vector $\bar{u} = [u_1, u_2, \dots u_{2*(N+1)}]^\intercal$ ($\Sigma_i u_i = 1$), where:

$$u_i = \begin{cases} Probability(S_{i-1}, OFF) \text{ with } i \leq N+1 \\ Probability(S_{i-1}, ON) \text{ with } i > N+1. \end{cases} \quad (5)$$

At $t = 0$, we assume that all the Bcd binding sites are free, and the promoter is OFF. Therefore, we have the initial condition: $\overline{u_0} = [u_1 = 1, u_{i>1} = 0]^\intercal$.

As all the transitions between promoter and binding array states are first-order reactions, the system dynamics can be described by a 2N+2 by 2N+2 transition matrix A with elements $[a_{ij}]$.

The binding reaction (from S_i to S_{i+1}) is modeled by:

$$a_{i,i+1} = a_{i+N+1,i+N+2} = k_i[Bcd] \text{ with } i \leq N. \quad (6)$$

In Eq. 6,$[Bcd]\sim e^{-x/\lambda}$ is the Bcd concentration, which can be calculated from the nuclei position x and the decay length of the Bcd gradient λ.

The unbinding reaction (from S_{i+1} to S_i) is modeled by:

$$a_{i+1,i} = a_{i+N+2,i+N+i} = k_{-i} \text{ with } 1 < i \leq N+1. \quad (7)$$

The activation of the promoter (from OFF state to ON state) is given by:

$$a_{i,i+N+1} = k_{ON}(i-1, K) \text{ with } i \leq N+1, \quad (8)$$

where the turning ON rate $k_{ON}(i, K)$ is modulated by i the number of bound Bcd molecules. $k_{ON}(i < K, K) = 0$.

The deactivation of the promoter (from ON state to OFF state) is given by:

$$a_{i+N+1,i} = k_{OFF} \text{ with } i \leq N+1. \quad (9)$$

To balance the transition matrix, we set the diagonal elements as:

$$a_{i,i} = -\Sigma_j a_{i,k} \text{ with } j \neq i. \quad (10)$$

With the transition matrix defined, we can calculate the probability vector at a given time t:

$$\bar{u}(t) = e^{-At}\bar{u}_0. \tag{11}$$

The probability of the promoter to be ON is given by:

$$P_{ON}(t) = \bar{v}^{\mathbf{T}}\,\bar{u}(t), \tag{12}$$

in which $\bar{v} = [v_i]$ is the emission vector specifying the ON state with $v_i = 1$ with $i > N + 1$ and 0 otherwise.

E. Calculating the shift in pattern along AP axis

In this section, we present a framework to quantify the shift of the *ms2* expression patterns along the AP axis from Bcd-2x to Bcd-1x flies.

We define two random variables F and G as the gene expression level in Bcd-2X and Bcd-1X embryos, respectively. Given that the experiments in Bcd-2X and Bcd-1X are independent, the probability distribution of F and G are independent. X and S are the nuclei position in Bcd-2X and Bcd-1X respectively, and are described by a uniform distribution from -50 %EL to 50 %EL. At any given position x and s in the embryo, $P_{F|X}$ $(F|X = x)$ and $P_{G|S}$ $(G|S = s)$ are assumed to be Gaussian distributed, with the mean and standard deviation equal to the mean and standard error of expression levels (either fraction of expressing nuclei (Fig. 1D).

We call R the nuclei position in Bcd-1X that has the same expression level as in the nuclei at position X in Bcd-2X. The conditional distribution $P_{R|X}$ $(R\,|X = x)$ is given by:

$$\begin{aligned} P_{R|X}(R = s|X = x) &= \int_{-\infty}^{\infty}\int_{-\infty}^{\infty} df\, dg\, P_{FGS|X}(f, g, s|x)\, \delta(f - g) \\ &= \int_{-\infty}^{\infty}\int_{-\infty}^{\infty} df\, dg\, P_{F|X}(f|x)P_{G|X}(g|s)P_S(s)\, \delta(f - g) \\ &= \int_{\infty}^{\infty} df\, P_{F|X}(f|x)P_{G|S}(f|s)P_S(s). \end{aligned} \tag{13}$$

In Eq. 13, $\delta(f - g)$ is a Dirac delta function taking non-zero value only when the expression level in Bcd-2X and Bcd-1X are equal $f = g$. As the nuclei position S is uniformly distributed from -50 %EL to 50 %EL, $P_S(s)$ is constant and equal to $(\%EL)^{-1}$.

We denote by $\mu_f(x)$ and $\mu_g(s)$ the mean, $\sigma_f(x)$ and $\sigma_g(s)$ the standard deviation of $P_{F|X}(F|X = x)$ and $P_{G|S}(G|S = s)$ respectively.

$$\begin{aligned} P_{F|X}(f|x) &= \frac{1}{\sqrt{2\pi\sigma_f^2}} e^{-\frac{\left(f-\mu_f(x)\right)^2}{2\sigma_f^2(x)}}, \\ P_{G|S}(f|s) &= \frac{1}{\sqrt{2\pi\sigma_g^2}} e^{-\frac{\left(f-\mu_g(s)\right)^2}{2\sigma_g^2(s)}}. \end{aligned} \tag{14}$$

Eq. 13 can be rewritten as (suppressing the explicit x and s dependence):

$$P_{R|X}(R = s|X = x) \sim \int_{\infty}^{\infty} df \frac{1}{\sqrt{2\pi 2\pi\sigma_f^2\sigma_g^2}} e^{-\frac{\left(f-\mu_f\right)^2}{2\sigma_f^2} - \frac{(f-\mu_g)^2}{2\sigma_g^2}} = e^{-C/2}, \tag{15}$$

with the term C given by:

$$C = \frac{1}{\sigma_f^2+\sigma_g^2}\left(\mu_f - \mu_g\right)^2 + \ln(2\pi(\sigma_f^2 + \sigma_g^2). \tag{16}$$

From Eq. 15 and Eq. 16, we can analytically calculate the probability $P_{R|X}(s|x)$ for each pair of position x and s from the mean and standard error of gene expression level at a given position.

The probability distribution of the shift $\Delta(x)$ from position x to position $P_{R|X}(R|X=x)$ is given by:

$$P_{\Delta(x)}(\Delta|x) = P_{R|X}(R = x + \Delta|x). \quad (17)$$

Given this probability distribution $P_{\Delta(x)}(\Delta)$ as a function of x, we can find a constant value of the shift $\Delta(x) = \tilde{\Delta}$ that best describes the observed shift for all positions x within ϵX:

$$\tilde{\Delta} = \arg\max_{\Delta} \int_{\epsilon X} \mathrm{p}(\Delta(\mathrm{x}) = \Delta)\, dx. \quad (18)$$

F. Fitting the models of transcription regulation by Bcd

We fit the models of Bcd binding/unbinding to binding sites and activation of transcription, each with a different value of the Bcd gradient decay length λ, to the transcription dynamics by the synthetic reporters (Fig. 2 and Fig. S4) and hb-P2 reporter (Fig. 5).

Data

The data used for the fitting is the fraction of active loci $P_{Spot}(j,t,x)$ at a given time t and position x along the AP axis (observed from -30 %EL to 20 %EL) in the jth embryo (of total *n* embryos). t ranges from 600 to 800s into nc13 for synthetic reporters and from 0 s to 800 s into nc13 for hb-P2.

We discretize the time axis to increments of 10 s and nuclei position to increments of 1 %EL.

Parameter constraints

i) Number of binding sites N

The model used in the fitting is described in the Results section and Fig. 2D-E of the main text. The number of Bcd binding sites is $N = 6$ for B6, H6B6, Z2B6 and hb-P2 (Driever and Nusslein-Volhard, 1988), $N = 9$ for B9 and $N = 12$ for B12.

ii) Bcd search rate constant for a target binding site k_b

The Bcd gradient follows an exponential gradient with a predefined decay length λ:

$$[Bcd] = c_A e^{-(x-x_A)/\lambda}, \quad (19)$$

with c_A chosen to be 140 nM or 84 molecules/μm^3 (Abu-Arish et al., 2010). x_A, which is -35 %EL, is the nuclei position where the Bcd gradient plateaus (Gregor et al., 2007b; Houchmandzadeh et al., 2002; Liu et al., 2013).

Unless otherwise specified, we assume that Bcd molecules independently diffuse in the 3D nuclear space in search for the target sites of the reporters and that the binding to the sites is diffusion limited. Therefore, the binding rate k_i of Bcd to the binding site array depends on the number of free binding sites:

$$k_i = (N - i)k_b. \quad (20)$$

Here, k_b is the binding rate constant of individual Bcd molecule to a single target site and equal $(\tau_{bind}.[Bcd])^{-1}$ (see Eq. 33 below). The diffusion coefficient is taken to be D=4.6 μm^2/s and the target size a=3nm (Abu-Arish et al., 2010). Therefore, k_b=5.52 μm^3/s.

iii) Bcd unbinding rate constants k_{-i}

There are no constraints on the unbinding rate constants k_{-i} of Bcd from the target binding array. However, for simplicity, we assume only two forms of Bcd binding cooperativity: bi-cooperativity and 6-cooperativity. It is found from (Tran et al., 2018a) that these two forms of cooperativity are sufficient to generate regulation functions of any order (Hill coefficient H between 1 and 6) within the physical limit without extra energy expenditure (Estrada et al., 2016). Therefore, we use three free parameters k_{-1}, k_{-2} and k_{-6} to describe k_{-i}. Assuming at state $S_{-(1<i<6)}$, bound Bcd can unbind independently from the BS array, the intermediate binding rates are given by:

$$k_{-(1<i<6)} = i.k_{-2}/2, \tag{21}$$

iv) Promoter switching rates $k_{ON}(S_i)$ and k_{OFF}

For the promoter activation and deactivation rates when bound by enough Bcd ($k_{ON}(S_i)$ and k_{OFF}), we adopt the scheme of the formation of transient "K-mer" (Fig. S2C) as it can explain the big fold change in the activation rate between $k_{ON}(S_6)$, $k_{ON}(S_9)$ and $k_{ON}(S_{12})$. From Table S3, K is chosen to be 3.

$$k_{ON}(S_i) = \begin{bmatrix} i \\ K \end{bmatrix} k_{ON}(S_K) = k_{ON}(S_6) \begin{bmatrix} i \\ 3 \end{bmatrix} / \begin{bmatrix} 6 \\ 3 \end{bmatrix}. \tag{22}$$

In summary, for the fitting of synthetic reporters' patterns at steady state (Fig. 2E-G and 4), the possible free parameters, with the corresponding ranges of values, are:

- Binding rate constants: k_b with range [e^{-20} /s, e^{20} /s].
- The minimal number of Bcd to activate transcription K with integer range [1,6]
- Unbinding rate constants: k_{-1}, k_{-2}, k_{-6} with range [e^{-20} /s, e^{20} /s]
- Activation and deactivation rate constants with K bound Bcd molecules: $k_{ON}(S_K)$ and k_{OFF} with range [0.001 /s,100 /s]

For the fitting of hb-P2 pattern dynamics during nc13 (Fig. 5), the free parameters, with the corresponding ranges of values, are:

- Unbinding rate constants: k_{-1}, k_{-2}, k_{-6} with range [e^{-20} s, e^{20} s]
- Activation and deactivation rate constants with K bound Bcd molecules: $k_{ON}(S_K)$ and k_{OFF} with range [0.001 /s,100 /s]

Additionally, when fitting hb-P2 pattern, we also fit the offset time t_{offset}>0 as the first time Bcd molecules are allowed to interact with target binding sites following mitosis.

Objective function

For each set of parameter $\phi = [k_b, k_{-1}, k_{-2}, k_{-6}, K, k_{ON}(S_6), k_{OFF}, t_{offset}]$, we calculate all the model rate constants k_i, k_{-i}, $k_{ON}(S_i)$, k_{OFF} according to Fig. S2 and Eq. 20-22. At a given nuclei position x, the Bcd concentration $[Bcd]$ is given by Eq. 19. Given that all the reactions in the model (Fig. 2) are first order, the system dynamics at nuclei position x can be described by a transition matrix $A(x)$. We can predict the fraction of nuclei in the active state $P_{ON}(t,x)$ at any given time t and nuclei position x (see section D).

The objective function is given by the sum of squared errors from all *n* embryos:

$$obj(\phi) = \Sigma_{j=1..n}\left(P_{ON}\left(t - t_{offset}, x\right) - P_{Spot}(j,t,x)\right)^2. \quad (23)$$

Parameter estimation

The best fit parameter set $\bar{\phi}$ is given by minimizing the objective function:

$$\bar{\phi} = argmin_{\phi}\, obj(\phi). \quad (24)$$

In practice, we first generate ~2000 randomized initial values for the parameter set ϕ within the preset value ranges. For each initial value, we perform zeroth-order minimization using simplex search method with MATLAB's *fminsearch* function (Lagarias et al., 1998) to find the local minima. The best fit parameter set $\bar{\phi}$ is set corresponding to smallest local minimum.

QUANTIFICATION AND STATISTICAL ANALYSIS

G. Evidence for synergistic activation between several bound Bcd molecules

In the anterior region, we assume the binding array is always fully bound by Bcd. Thus, in our model, for a synthetic reporter B_N with N Bcd sites (N=3,6,9,12), the binding array state spends most of the time at state S_N. Because the MS2 stem-loops are placed at the 3' end of the transcribed sequence, we assume a negligible travel time of transcribing RNAP from the beginning of the first stem-loop to the terminator site (Fukaya et al., 2017). Thus, we approximate the probability of the promoter being in the ON state with the fraction of *ms2* loci active time (bright MCP-GFP spots observed) at steady state:

$$P_{Spot}(B_N) = P_{ON}(S_N) = \frac{k_{ON}(S_N)}{k_{ON}(S_N)+k_{OFF}}. \quad (25)$$

We can calculate the activation rate $k_{ON}(S_N)$ as:

$$k_{ON}(S_N) = (k_{ON}(S_N) + k_{OFF})P_{Spot}(B_N), \quad (26)$$

$$k_{ON}(S_N) = k_{OFF}\frac{P_{Spot}(B_N)}{1-P_{Spot}(B_N)}. \quad (27)$$

With $P_{Spot}(B_N)$ observed from the data (N=6, 9, 12), the fold change in the activation rates between B6, B9 and B12 is found to be:

$$\frac{k_{ON}(B9)}{k_{ON}(B6)} = \frac{P_{Spot}(B9)(1-P_{Spot}(B6)}{P_{Spot}(B6)(1-P_{Spot}(B9)} = \frac{0.8*(1-0.47)}{(1-0.8)*0.47} \approx 4.51, \quad (28)$$

$$\frac{k_{ON}(B12)}{k_{ON}(B6)} = \frac{P_{Spot}(B12)(1-P_{Spot}(B6)}{P_{Spot}(B6)(1-P_{Spot}(B12)} = \frac{0.8*(1-0.47)}{(1-0.8)*0.47} \approx 4.51. \quad (29)$$

This fold change between $k_{ON}(S_9)$ to $k_{ON}(S_6)$, which is 3 times greater than the ratio of the Bcd BS numbers between B9 and B6, argues against independent activation of transcription by individual bound Bcd TF, where the fold change scales with the number of BS ($K = 1$ and $k_{ON}(S_N) = N\, k_{ON}(S_1)$). Therefore, bound Bcd molecules are likely to cooperate with each other to activate transcription.

We considered various schemes of cooperative activation by bound Bcd and calculated the fold change in k_{ON} for different values of N and K (Fig. S2 and Table S3). Among the schemes considered, the fold change in k_{ON} from S_6 and S_9 was achieved only when bound Bcd can randomly form transient "K-mers" capable of activating transcription, and when K is between 3 and 6.

However, the schemes with transient "K-mers" cannot explain the similar P_{Spot} value observed in the anterior region for B9 and B12 reporters. One possibility is that Bcd molecules bound to the distal BS in B12 are too far from the TSS to activate transcription and thus $k_{ON}(S_{12}) = k_{ON}(S_9)$. Another explanation is that $P_{Spot} \approx 0.8$ is the upper limit imposed by inherent bursty dynamics of transcription even when the activation by bound Bcd is instantaneous ($k_{ON}(S_{12}), k_{ON}(S_9) \gg k_{ON}(S_6)$). In any case, the value of $k_{ON}(S_9)/k_{ON}(S_6)$~4.5 calculated from the data should represent a lower bound for the

value of the fold change in the activation rates. Thus, our conclusions regarding the synergistic activation by bound Bcd molecules still hold.

Note that, in the alternative model, where the Bcd-DNA complex S_i regulates the deactivation rate $k_{OFF}(S_i)$ but not the activation rate k_{ON}. The ratio between k_{ON} and $k_{OFF}(S_i)$ still holds, as in Eq. 28 and 29. The fold change in the deactivation rates between B6, B9 and B12 is:

$$\frac{k_{OFF}(B9)}{k_{OFF}(B6)} = \frac{P_{Spot}(B6)(1-P_{Spot}(B9)}{P_{Spot}(B9)(1-P_{Spot}(B6)} = \frac{0.47*(1-0.8)}{(1-0.47)*0.8} \approx 0.22, \quad (30)$$

$$\frac{k_{OFF}(B12)}{k_{OFF}(B6)} = \frac{P_{Spot}(B6)(1-P_{Spot}(B12)}{P_{Spot}(B12)(1-P_{Spot}(B6)} = \frac{0.47*(1-0.8)}{(1-0.47)*0.8} \approx 0.22. \quad (31)$$

H. Bicoid search time for its target sites

We recalculate the Bcd search time for its target site at the critical *hb* expression boundary (~-5 %EL) with different values of the Bcd gradient decay length λ. The Bcd gradient follows an exponential gradient with a fixed concentration at the anterior c_A:

$$[Bcd] = c_A e^{-(x-x_A)/\lambda}, \quad (32)$$

where $[Bcd]$ is the Bcd concentration at a given nuclei position of distance x away from the anterior pole (x_A). As Bcd concentration peaks at -35 %EL (Gregor et al., 2007a; Houchmandzadeh et al., 2002), x_A is set to be -35 %EL.

We assume that each Bcd molecule searches for its target sites via 3D diffusion in the nuclear space, with a diffusion coefficient D. Each target site has a size of a. If the binding of Bcd to the target site is diffusion limited, the Bcd search time for individual target sites τ_{bind} at a given position x is given by:

$$t_{bind} \sim \left(Dac_A e^{-(x-x_A)/\lambda}\right)^{-1}. \quad (33)$$

From Eq. 33, it can be seen that the search time t_{bind} is longer with decreasing λ.

In practice, there are many uncertainties regarding the exact values of c_A, D and a, making it difficult to estimate t_{bind} (See Table S4 for details).

If the target gene can sense the Bcd concentration via N=6 identical and independent binding sites, we calculate the minimum observation time T it takes to achieve the prediction error $\delta[Bcd]/[Bcd]$ = 10 % of the Bcd concentration at the hb-P2 boundary (x = -5 %EL) in the Berg and Purcell limit (Berg and Purcell, 1977):

$$\frac{\delta[Bcd]}{[Bcd]} = \sqrt{\frac{1}{NTDac_A e^{-(x-x_A)/\lambda}}}, \quad (34)$$

$$T = \left(\frac{\delta[Bcd]}{[Bcd]}\right)^{-2} \frac{1}{NDac_A e^{-(x-x_A)/\lambda}} = \frac{16.7}{Dac_A e^{-30/\lambda}}. \quad (35)$$

We compare the target site search time t_{bind} and the minimum required readout time T with λ equal 12 %EL and 20 %EL in Table S5. We consider different combinatory values of c_A, D and a found in Table S4.

Table S1

Name	Sequence
hb-P2 (*hb* intron included)	CTGTCGACTCCTGACCAACGTAATCCCCATAGAAAACCGGTGGAAAATTCGCAGCTCGCTGCTA AGCTGGCCATCCGCTAAGCTCCCGGATCATCCAAATCCAAGTGCGCATAATTTTTTGTTTCTGCT CTAATCCAGAATGGATCAAGAGCGCAATCCTCAATCCGCGATCCGTGATCCTCGATTCCCGACC GATCCGCGACCTGTACCTGACTTCCCGTCACCTCTGCCCATCTAATCCCTTGACGCGTGCATCCG TCTACCTGAGCGA**TATATAAA**CTAATGCCTGTTGCAATTGTTCAGTCAGTCACGAGTTTGTTAC CACTGCGACAACACAACAGAAGCAGCACCAATAATATACTTGCAAATCCTTACGAAAATCCCGA CAAATTTGGAATATACTTCGATACAATCGCAATCATACGCACTGAGCGGCCACGAAACGGTAG GATATTGTTAGCCATTACCAAGTGTCTCCATTTTGAACACAAAATCACTCAAATCGCCTTCAGGG GGTGGGTGCCGCCCAGCCACCCCTGACGTATTTTTTGTTAGGGGTGGTGCCGCAAGCACACCA AAAAAAGAGAAAAAAAAAATAAAAGCGAGGAAAAATAAAATGAAAAACAAGCGGAAAAAAA GAGGAAAAAACTCGACGCAGGCGCAGTGCATGAATGAATAAATGAATATGCCCACTAACCCCA CTCTCTCTGTTTTCTTATCCATTACAGCCGTCTAGAGCCGCCAAGG
iRFP	ATGGCGCGTAAGGTCGATCTCACCTCCTGCGATCGCGAGCCGATCCACATCCCCGGCAGCATTC AGCCGTGCGGCTGTCTCCTAGCCTGCGACGCGCAGGCGGTGCGGATCACGCGCATTACGGAA AATGCCGGCGCGTTCTTTGGACGCGAAACTCCGCGGGTCGGTGAGCTACTCGCCGATTACTTC GGCGAGACCGAAGCCCATGCGCTGCGCAACGCACTGGCGCAGTCCTCCGATCCAAAGCGACC GGCGCTGATCTTCGGTTGGCGCGACGGCCTGACCGGCCGCACCTTCGACATCTCACTGCATCG CCATGACGGTACATCGATCATCGAGTTCGAGCCTGCGGCGGCCGAACAGGCCGACAATCCGCT GCGGCTGACGCGGCAGATCATCGCGCGCACCAAAGAACTGAAGTCGCTCGAAGAGATGGCCG CACGGGTGCCGCGCTATCTGCAGGCGATGCTCGGCTATCACCGCGTGATGTTGTACCGCTTCG CGGACGACGGCTCCGGGATGGTGATCGGCGAGGCGAAGCGCAGCGACCTCGAGAGCTTTCTC GGTCAGCACTTTCCGGCGTCGCTGGTCCCGCAGCAGGCGCGGCTACTGTACTTGAAGAACGCG ATCCGCGTGGTCTCGGATTCGCGCGGCATCAGCAGCCGGATCGTGCCCGAGCACGACGCCTCC GGCGCCGCGCTCGATCTGTCGTTCGCGCACCTGCGCAGCATCTCGCCCTGCCATCTCGAATTTC TGCGGAACATGGGCGTCAGCGCCTCGATGTCGCTGTCGATCATCATTGACGGCACGCTATGGG GATTGATCATCTGTCATCATTACGAGCCGCGTGCCGTGCCGATGGCGCAGCGCGTCGCGGCCG AAATGTTCGCCGACTTCTTATCGCTGCACTTCACCGCCGCCCACCACCAACGCTAA
MS2	GGATCCTACGGTACTTATTGCCAAGAAAGCACGAGCATCAGCCGTGCCTCAATGTCGAATCTGC AAACGACGACGATCACGCGTCGCTCCAGTATTCCAGGGTTCATCAGATCCTACGGTACTTATTG CCAAGAAAGCACGAGCATCAGCCGTGCCTCAATGTCGAATCTGCAAACGACGACGATCACGCG TCGCTCCAGTATTCCAGGGTTCATCAGATCCTACGGTACTTATTGCCAAGAAAGCACGAGCATC AGCCGTGCCTCAATGTCGAATCTGCAAACGACGACGATCACGCGTCGCTCCAGTATTCCAGGG TTCATCAGATCCTACGGTACTTATTGCCAAGAAAGCACGAGCATCAGCCGTGCCTCAATGTCGA ATCTGCAAACGACGACGATCACGCGTCGCTCCAGTATTCCAGGGTTCATCAGATCCTACGGTAC TTATTGCCAAGAAAGCACGAGCATCAGCCGTGCCTCAATGTCGAATCTGCAAACGACGACGAT CACGCGTCGCTCCAGTATTCCAGGGTTCATCAGATCCTACGGTACTTATTGCCAAGAAAGCACG AGCATCAGCCGTGCCTCAATGTCGAATCTGCAAACGACGACGATCACGCGTCGCTCCAGTATTC CAGGGTTCATCAGATCCTACGGTACTTATTGCCAAGAAAGCACGAGCATCAGCCGTGCCTCAAT GTCGAATCTGCAAACGACGACGATCACGCGTCGCTCCAGTATTCCAGGGTTCATCAGATCCTAC GGTACTTATTGCCAAGAAAGCACGAGCATCAGCCGTGCCTCAATGTCGAATCTGCAAACGACG

	ACGATCACGCGTCGCTCCAGTATTCCAGGGTTCATCAGATCCTACGGTACTTATTGCCAAGAAA GCACGAGCATCAGCCGTGCCTCAATGTCGAATCTGCAAACGACGACGATCACGCGTCGCTCCA GTATTCCAGGGTTCATCAGATCCTACGGTACTTATTGCCAAGAAAGCACGAGCATCAGCCGTGC CTCAATGTCGAATCTGCAAACGACGACGATCACGCGTCGCTCCAGTATTCCAGGGTTCATCAGA TCCTACGGTACTTATTGCCAAGAAAGCACGAGCATCAGCCGTGCCTCAATGTCGAATCTGCAAA CGACGACGATCACGCGTCGCTCCAGTATTCCAGGGTTCATCAGATCCTACGGTACTTATTGCCA AGAAAGCACGAGCATCAGCCGTGCCTCAATGTCGAATCTGCAAACGACGACGATCACGCGTCG CTCCAGTATTCCAGGGTTCATCAGATCC
HSBG promoter	ACCGCCGGAG**TATAAATA**GAGGCGCTTCGTCTACGGAGCGACAATTCAATTCAAACAAG**C**AAA GTGAACACGTCGCTAAGCGAAAGCTAAGCAAATAAACAAGCGCAGCTGAACAAGCTAAACAA TCGGGGTACGGCTAGCA
B3	TCGACTCATGGGATTAGACTCGAGGGATTAGACCGGGATTAGAGGGATCCAAGCTTATCGATT TCGGCGCGCCCGTGACTGATCAGTCATGGATCCAAGCTTATCGATTTCGAACCCTCGACCGCCG GAG**TATAAATA**
B6	TCGACTCATGGGATTAGACTCGAGGGATTAGACCGGGATTAGAACCTGGGGATCGGGGATTA GACTCGAGGGATTAGACCGGGATTAGAGGATCCAAGCTTATCGATTTCGAACCCTCGACCGCC GGAG**TATAAATA**
B9	TCGACTCATGGGATTAGACTCGAGGGATTAGACCGGGATTAGAACCTGGGGATCGGGGATTA GACTCGAGGGATTAGACCGGGATTAGAGGATCCATGGGATTAGACTCGAGGGATTAGACCGG GATTAGAGGGATCCAAGCTTATCGATTTCGAACCCTCGACCGCCGGAG**TATAAATA**
B12	TCGACTCATGGGATTAGACTCGAGGGATTAGACCGGGATTAGAACCTGGGGATCGGGGATTA GACTCGAGGGATTAGACCGGGATTAGAGGATCCATGGGATTAGACTCGAGGGATTAGACCGG GATTAGAACCTGGGGATCGGGGATTAGACTCGAGGGATTAGACCGGGATTAGAGGGATCCAA GCTTATCGATTTCGAACCCTCGACCGCCGGAG**TATAAATA**
H6	TCGGTACCATAGTTTTTTGAGTATCGATAGTTTTTTGAGTCCATATTTTTTGAGTACTCATAGTTT TTTGAGTATCGATAGTTTTTTGAGTCCATATTTTTTGAGTGTCGACGGTATCGATAAGCGGATCC AAGCTTATCGATTTCGAACCCTCGACCGCCGGAG**TATAAATA**
H6B6	TCGGTACCACTCAAAAAATATGGACTCAAAAAACTATCGATACTCAAAAAACTATGAGTACTCA AAAAATATGGACTCAAAAAACTATCGATACTCAAAAAACTATGGTACCGTACCCCGTCGACTCA TGGGATTAGACTCGAGGGATTAGACCGGGATTAGAACCTGGGGATCGGGGATTAGACTCGAG GGATTAGACCGGGATTAGAGGATCCAAGCTTATCGATTTCGAACCCTCGACCGCCGGAG**TATA AATA**
Z2	TCATGGATCTCAGGTAGTAACTGACCAGGTAGGAGGATCCAAGCTTATCGATTTCGAACCCTCG ACCGCCGGAG**TATAAATA**
Z2B6	TCATGGATCCAGGTAGTAACTGACCAGGTAGCTATGGTACCGTACCCCGTCGACTCATGGGATT AGACTCGAGGGATTAGACCGGGATTAGAACCTGGGGATCGGGGATTAGACTCGAGGGATTAG ACCGGGATTAGAGGATCCAAGCTTATCGATTTCGAACCCTCGACCGCCGGAG**TATAAATA**

Z6	TCATGGATCCAGGTAGATATCGCACAGGTAGCGATCATACAGGTAGCCTAGATCCAGGTAGTC AATGATCAGGTAGTAACTGACCAGGTAGGATCCAAGCTTATCGATTTCGAACCCTCGACCGCC GGAG**TATAAATA**
Oligo for 5' cut Fw	5'-GTCGGTCTAATTGATTCCTAAATT-3'
Oligo for 5' cut Rv	5'-AAACAATTTAGGAATCAATTAGAC-3'
Oligo for 3' cut Fw	5'-GTCGGAATGAACGAAAACAGTATC-3'
Oligo for 3' cut Rv	5'-AAACGATACTGTTTTCGTTCATTC-3'
Bcdnull_5 HR_fw	5'- TAAGAGACGTATAGGAGACCTATAGTGTCTTCGGGGCCGATTCGAAAACT TTCTGCTGCC-3'
Bcdnull_5 HR_rv	5'-TTTAACGTACGTCACAATATGATTATCTTTCTAGGGTTAATCAATTAGACAAGTG TCGAATGTTTAATTTG-3'
Bcdnull_D sRed_fw	5'- ACAAAAATTCAAATTAAACATTCGACACTTGTCTAATTGATTAACCCTAGAAA GATAATC-3'
Bcdnull_D sRed_rv	5'- ATTTTTAAATTCATAAGATTTTCGGGAAAACCAGATACTGTTAACCCTAG AAAGATAGTC-3'
Bcdnull_3 HR_fw	5'-GCGCGCTCTTCGTAACAGTATCTGGTTTTCCCGAA-3'
Bcdnull_3 HR_rv	5'-TATAGCTCTTCACGGCTGGTGAAGGCAGTCCGTGA-3'

Table S1. Promoter sequences of hb-P2, synthetic MS2 reporters and oligonucleotides required for generating the *Δbcd* molecular null allele. The sequences are shown in modules, as arranged in Fig. 1 in the main text. The TATA boxes of hb-P2 and HSBG promoter are highlighted in bold. In the binding array sequences, the binding sites for each protein are highlighted in grey (Bcd), green (Hb) and yellow (Zelda). For clarity, the binding array sequences are shown up to the TATA box of HSBG promoter.

Table S2.

	Fraction of expression nuclei			Fraction of active loci at steady state P_{Spot}		
	Boundary position (%EL)	Boundary width (%EL)	Converging time (s)	Boundary position (%EL)	Boundary width (%EL)	Pattern Sharpness $(\%EL)^{-1}$
hb-P2	-5.0 ± 0.3	11.0 ± 1.6	225 ± 25	-9.9 ± 0.4	16.8 ± 2.0	0.33 ± 0.04
B6	-12.9 ± 1.0	25.6 ± 3.6	425± 25	-15.6 ± 1.0	24.7 ± 5.6	0.22 ± 0.05
B9	-5.1 ± 0.4	17.6 ± 2.2	475± 25	-7.3 ± 0.5	18.9 ± 2.0	0.30 ± 0.07
B12	-4.2 ± 0.5	16.4 ± 2.5	325 ± 25	-6.0 ± 0.7	19.6 ± 6.9	0.29 ± 0.07
H6B6	-9.8 ± 0.4	13.8 ± 1.8	325 ± 25	-13.3 ± 0.4	18.9 ± 2.0	0.30 ± 0.03
Z2B6	-4.6 ± 0.7	19.4 ± 3.2	300 ± 25	-0.6 ± 1.4	19.6 ± 6.9	0.29 ± 0.12

Table S2. Position and width of the gene expression boundary based on fraction of expression nuclei feature (Fig. 1H and Fig. 3G in Main text) and fraction of active loci P_{spot} feature (Fig. 2A and Fig. 3H in Main text) in the steady window (600-800s into nc13) for hb-P2 and synthetic reporters in Bcd-2X, shown with 95% confidence interval. For the fraction of expression nuclei, also shown is the time to reach the final activation decision boundary (±2 %EL) starting from the detection the first spot (~225 s) after mitosis.

Table S3

Scheme	K	$\frac{k_{ON}(B9)}{k_{ON}(B6)}$	$\frac{k_{ON}(B12)}{k_{ON}(B6)}$
Independent activation $k_{ON}(S_i) = ik_{ON}(S_1)$	1	1.5	2
Formation of transient *K*-mer $k_{ON}(S_i) = \frac{i!}{K!\,(i-K)!}\ k_{ON}(S_K)$	1	1.5	2
	2	2.4	4.4
	3	4.2	**11**
	4	**8.4**	**33**
	5	**21**	**132**
	6	**84**	**924**
Formation of stable K-mer $k_{ON}(S_i) = k_{ON}(S_K)$	$0 \leq K \leq 6$	1	1

Table S3. Expected fold change in the activation rates in the anterior region (saturating Bcd concentration) $k_{ON}(S_{i=N})$ between B9 and B6 and between B12 and B6. The fold changes are shown for different schemes of activation and values of *K* (Fig. S2). The fold changes above the value calculated from the data (~4.51) are made bold.

Table S4

Parameters	Value	Note	Reference
c_A (molecules/µm^3)	~33	Imaging with Bcd-eGFP	(Gregor et al., 2007b)
	~84	Extract using Bcd-eGFP imaging and FCS	(Abu-Arish et al., 2010)
	~210	Comparison between immunostaining and imaging of Bcd-eGFP reveals ~ 2.5 time underestimation of Bcd concentration	(Liu et al., 2013)
D (µm^2/s)	<1	Imaging with Bcd-eGFP using FRAP	(Gregor et al., 2007a)
	~7.4	Diffusion coefficient of fast-diffusing Bcd population, extracted using FCS and Bcd-eGFP	(Abu-Arish et al., 2010)
	~4.6	Average diffusion coefficient, extract using FCS and Bcd-eGFP	(Abu-Arish et al., 2010)
a (nm)	3	Size for a single binding site of ~10bp	
	0.3	Size of a single nucleotide for exact match	

Table S4. Estimated values of Bcd concentration at the anterior (c_A), diffusion coefficient (D) and the size of the target for binding (a) from previous work.

Table S5

λ (%EL)	c_A (1/µm^3)	D (µm^2/s)	a (nm)	t_{bind} (s)	T (min)
15	33	7.4	3	26.9	7.5
			0.3	268.8	74.7
		4.6	3	43.2	12.0
			0.3	432.4	120.1
	84	7.4	3	10.6	2.9
			0.3	105.6	29.3
		4.6	3	17.0	4.7
			0.3	169.9	47.2
	210	7.4	3	4.2	1.2
			0.3	42.2	11.7
		4.6	3	6.8	1.9
			0.3	67.9	18.9
20	33	7.4	3	13.0	3.6
			0.3	129.5	36.0
		4.6	3	20.8	5.8
			0.3	208.3	57.9
	84	7.4	3	5.1	1.4
			0.3	50.9	14.1
		4.6	3	8.2	2.3
			0.3	81.8	22.7
	210	7.4	3	2.0	0.6
			0.3	20.4	5.7
		4.6	3	3.3	0.9
			0.3	32.7	9.1

Table S5. Bcd search time for the target site (t_{bind}) and the readout time (T) required for 10% error in Bcd concentration readout at hb-P2 boundary position (-4.9 %EL), calculated for different values of Bcd concentration at the anterior (c_A), diffusion coefficient (D) and targets size (a) in the Berg & Purcell limit (Berg and Purcell, 1977).

Figure S1

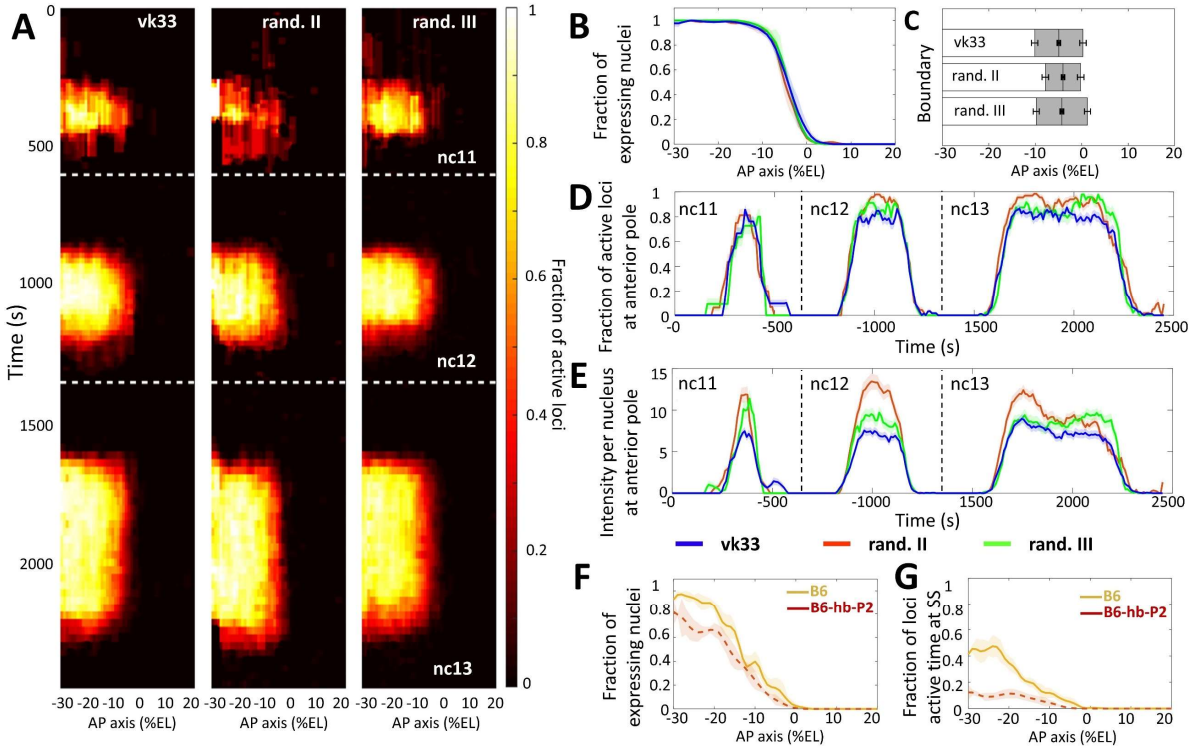

Figure S1. Comparison of transcription dynamics with hb-P2 reporters inserted at the vk33 site on the 3rd chromosome and randomly in the 2nd chromosome and 3rd chromosome (Lucas et al., 2018). **A**) Kymographs representing the fraction of nuclei with active *ms2* loci (represented as by the colormap) as a function of time and nuclei position along the AP axis. The white dashed horizontal lines represent mitoses between nuclear cycles. **B**) Fraction of nuclei with any *ms2* expression in nc13, averaged over multiple embryos, with shaded error of the mean as a function of nuclei position along AP axis (%EL). **C**) Bar plots with 95% confidence interval for the expression boundary position for ms2 reporters, based on the fraction of expressing loci (panel B). For each reporter, also shown is the boundary width as the grey region placed symmetrically around the boundary position. **D**) Time evolution of the fraction of active *ms2* loci near the anterior pole (from -35 to -25 %EL) in nc11, nc12 and nc13. **E**) Time evolution of the *ms2* locus intensity per nucleus at the anterior pole (from -35 to -25 %EL) in nc11, nc12 and nc13. In panel B, E and D, data is shown for the hb-P2 reporter inserted at the vk33 site (blue, n=5 embryos), randomly in the 2nd chromosome (red, n=3) and in the 3rd chromosome (green, n=6). **F**) Fraction of nuclei with *ms2* expression, averaged over multiple embryos, with shaded standard error of the mean, during nc13 along the AP axis (%EL). **G**) Fraction of *ms2* loci active time at steady state, averaged over multiple embryos, with shaded standard error of the mean, during nc13 along the AP axis (%EL). In panel F and G, data shown for B6 reporters with TATA box of HSBG promoter (solid orange) and of hb-P2 promoter (dashed red).

Figure S2

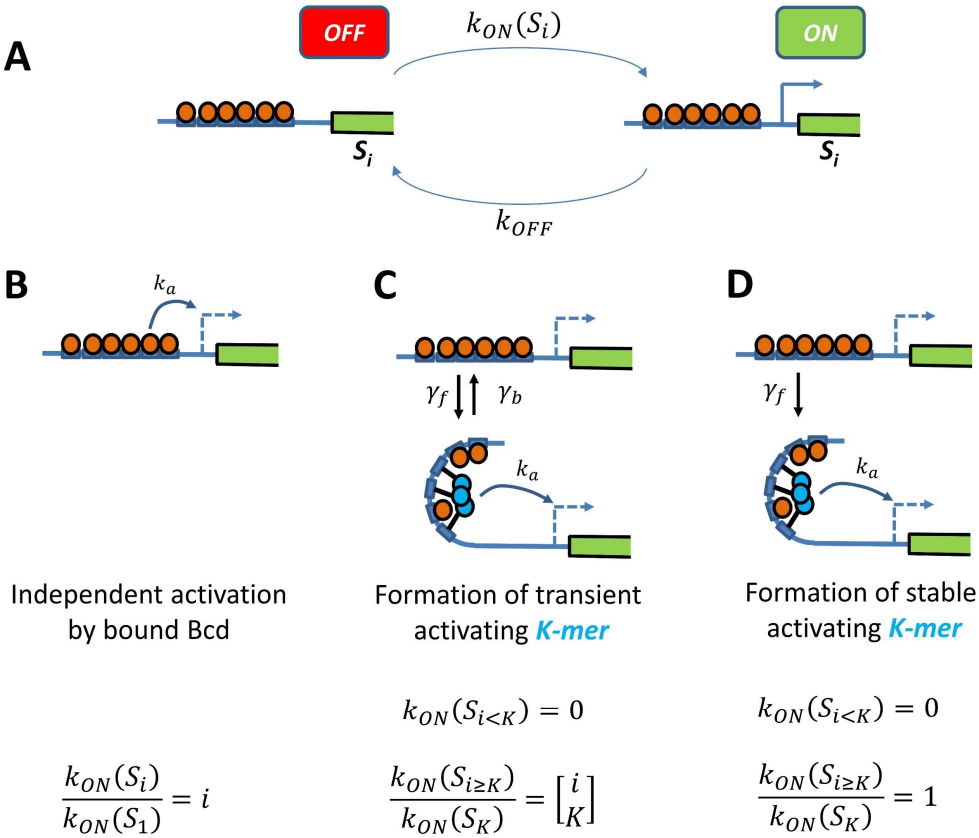

Figure S2. Schemes of transcription activation by bound Bcd molecules:
A) Context: When the binding sites are occupied by *i* Bcd molecules, the promoter can switch between two transcriptional states ON and OFF. The activation rate $k_{ON}(S_i)$, not the deactivation rate k_{OFF}, depends on the binding state S_i and how it interacts with the promoter (see schemes in panel B, C and D). **B**) Independent activation: Bound Bcd molecules (orange balls) can independently activate transcription at rate k_a. Activation can be enabled with even a single bound Bcd: $k_{ON}(S_1) = k_a$. The activation rate with binding state S_i is proportional to the number of bound Bcd: $k_{ON}(S_i)/k_{ON}(S_1) = i$. **C-D**) Formation of a stable activating "*K*-mer": Bound Bcd molecules (orange balls) can randomly form protein complexes (cyan balls) containing K molecules (hence called "*K*-mers"), which can activate transcription at rate k_a. There is no activation of transcription with less than *K* bound Bcd ($k_{ON}(S_{i<K}) = 0$). In panel C, The "*K*-mer" is constantly formed and degraded at rates γ_f and γ_b respectively. Assuming that these rates are fast enough (so that the formation and degradation of "*K*-mers" are always in equilibrium) and that $\gamma_b \ll \gamma_f$, the fold change in the activation rate is given by the number of ways to choose a subset of *K* molecules from *i* bound Bcd: $\frac{k_{ON}(S_i)}{k_{ON}(S_K)} = \left[\frac{i}{K}\right] = \frac{i!}{K!(i-K)!}$. In panel D, the protein complex is stable once formed ($\gamma_b = 0$). Assuming a negligible formation time when enough Bcd is bound ($1/\gamma_f \approx 0$), the activation rate is always constant $k_{ON}(S_{i\geq K}) = k_a$.

Figure S3

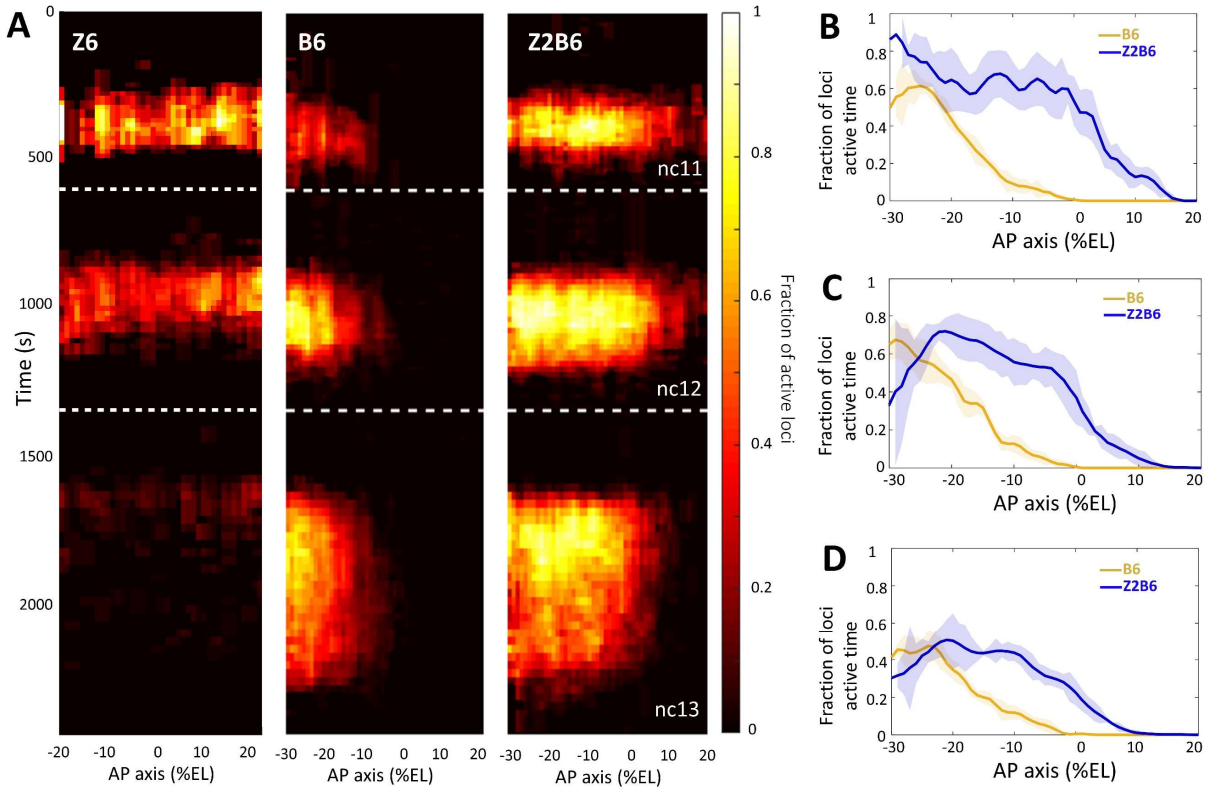

Figure S3. Transcription dynamics of the Z6 reporter (n=2 embryos), B6 (n=5 embryos) and Z2B6 (n=3 embryos) expression patterns

A) Kymographs representing the fraction of nuclei with active *ms2* loci (represented by the colormap) as a function of time and nuclei position along the AP axis. The white dashed horizontal lines represent mitoses between nuclear cycles. **B-D**) Comparison of B6 (orange) and Z2B6 (blue) patterns based on the fraction of loci active time, averaged over multiple embryos, with shaded standard error of the mean, in different time windows: (B) 450s-550s into nc12, (C) 450s-550s into nc13 and (D) 700s-800s into nc13.

Figure S4

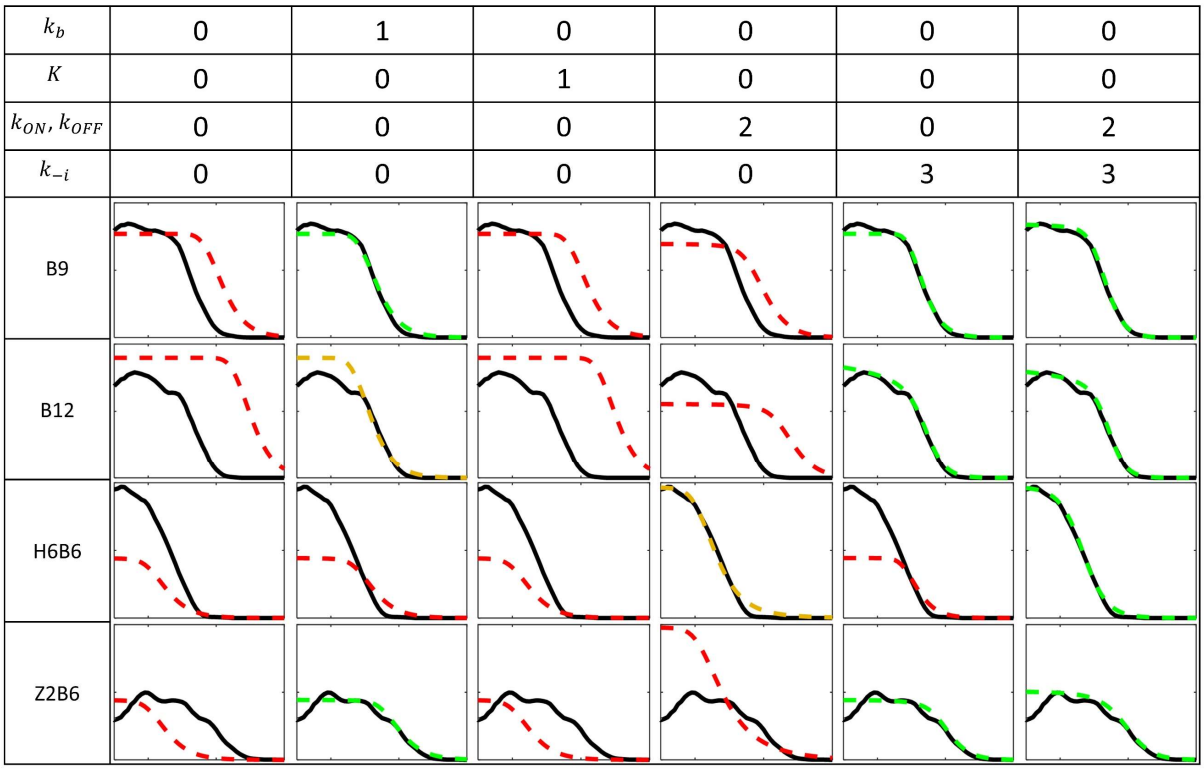

Figure S4. Fitting models to experimental data for the B9, B12, Z2B6 and H6B6 with the least degree of freedom when compared to B6: Each column corresponds to a fitting configuration with the number indicating the degree of freedom from the fitted B6 model for each group of kinetic parameters. A value of 0 indicates that the value of the kinetic parameter is imposed from the fitted model of B6 pattern (Fig. 2E). Parameters include the Bcd binding rate constant k_b, the minimal number of bound Bcd for transcription activation K, the promoter switching rate when bound by K Bcd molecules $k_{ON}(S_K)$ and k_{OFF}, and the unbinding rate constants of Bcd from the BS array k_{-i} (see Material & Method section F). The switching ON rates at higher bound states are set to $k_{ON}(S_{i>K}) = k_{ON}(S_K)[\frac{i}{K}]$, given the synergistic activation of transcription by bound Bcd (see Material & Method section G). For each fitting configuration and reporter are shown the patterns from the data (solid black) and from the fitted model (dashed color). On the y axis: fraction of loci active time at steady state (from 0 to 1). On the x axis: position along the AP axis (from -30 to 20 %EL). The quality of the model fit to the data (visually determined) is indicated by the color of the dashed curves as follow: good (green), moderate (orange) and red (bad).

Figure S5

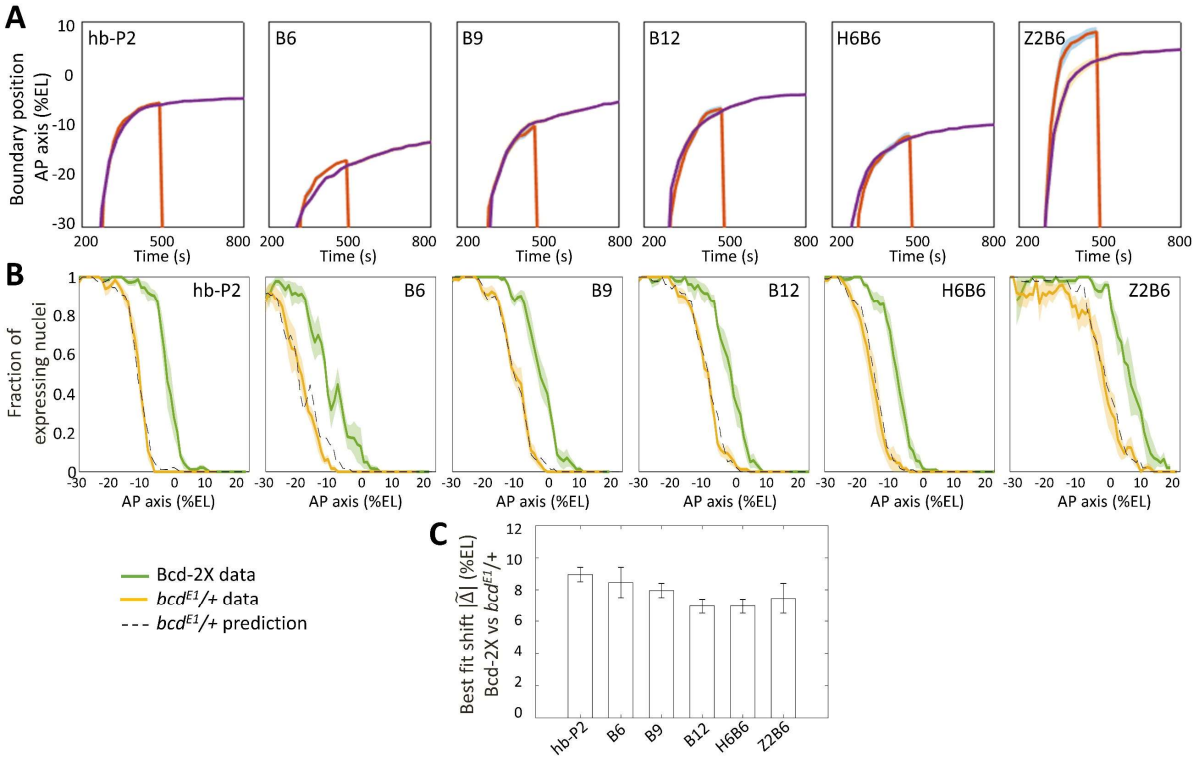

Figure S5. Comparison of fraction of expressing nuclei between nuclear cycles and between Bcd-2X and bcdE1/+ flies.

A) Boundary position of fraction of expressing nuclei along AP axis as a function time in nc12 (red) and nc13 (purple), shown for hb-P2 and synthetic reporters, shown with 95% confidence interval. The hb-P2 reporter reach position of expression boundary very rapidly therefore, the position of the boundary is the same at nc12 and nc13 for the hb-P2 reporter even though nc12 is very short. In contrast, positions of the Bcd-only reporters are different at the end of nc12 and nc13. This also true for H6B6 and Z2B6. **B**) Expression patterns of hb-P2 and synthetic reporters in embryos from wild-type (Bcd-2X, solid green lines with shaded errors) and *bcd*^{E1}/+ (solid yellow lines with shaded errors) females. Projection of *bcd*^{E1}/+ pattern (black dashed) from the Bcd-2X pattern assuming a fitted constant shift $\tilde{\Delta}$ = 9.0±0.5 %EL for hb-P2 (n_{2x} = 5 embryos, $n_{bcdE1/+}$ = 4 embryos), $\tilde{\Delta}$ = 8.5±1.0 %EL for B6 (n_{2x} = 5, $n_{bcdE1/+}$ = 4), $\tilde{\Delta}$ = 8.0±0.5 %EL for B9 (n_{2x} = 6, $n_{bcdE1/+}$ = 6), $\tilde{\Delta}$ = 7.0±0.5 %EL for B12 (n_{2x} = 4, $n_{bcdE1/+}$ = 6), $\tilde{\Delta}$ = 7.0±0.5 %EL for H6B6 (n_{2x} = 7, $n_{bcdE1/+}$ = 5), $\tilde{\Delta}$ = 7.5±1.0 %EL for Z2B6 (n_{2x} = 3, $n_{bcdE1/+}$ = 5). **C**) Comparison of the best fitted shift constant from Bcd-2X to *bcd*^{E1}/+ flies for hb-P2 and synthetic reporters.